University of La Laguna

Department of Physics

Master's Thesis in Astrophysics

The Electronic Structure of H_3^+, H_3 and H_3^- analyzed with NWChem Quantum Chemistry Package and Hückel's Model

---

Author:
Maren Brauner

Supervised by:
Dr. José Diego Bretón Peña
Dr. Javier Hernández Rojas

September 7, 2021

Acknowledgements

I would like to thank my supervisors for their constant support and dedication. I also thank the Department of Physics of the ULL for providing the NWChem Software.

Contents

Acknowledgements i

Resumen iii

1 Introduction 1
- 1.1 Historical Facts and Astrophysical Motivation . . . 1
- 1.2 Objectives . . . 2

2 Theoretical Background 4
- 2.1 Hartree-Fock (HF) self-consistent field (SCF) Method . . . 4
- 2.2 Post-Hartree-Fock Methods . . . 7
  - 2.2.1 Møller-Plesset second order perturbation theory (HF-MP2) . . . 7
  - 2.2.2 Coupled Cluster (CC) . . . 9
- 2.3 Basis sets . . . 11
- 2.4 Hückel Molecular Orbital (HMO) Model . . . 12

3 NWChem Software 14

4 Results and Discussion 16
- 4.1 Trihydrogen cation H_3^+ . . . 17
  - 4.1.1 Electronic Structure and Potential Energy Curves (PECs) . . . 17
  - 4.1.2 Application of the HMO Model . . . 20
  - Electron density . . . 22
- 4.2 Trihydrogen H_3 . . . 25
  - 4.2.1 Electronic Structure and Potential Energy Curves (PECs) . . . 25
  - 4.2.2 Application of the HMO Model . . . 27
- 4.3 Trihydrogen anion H_3^- . . . 30
  - 4.3.1 Electronic Structure and Potential Energy Curves (PECs) . . . 30
  - 4.3.2 Application of the HMO Model . . . 33
  - Electron density . . . 34

5 Conclusions 38

A Sample Input File 40

Bibliography 41

Resumen

Esta tesis trata sobre la estructura electrónica de las moléculas H_3^+, H_3 y H_3^-. Se centra en el cálculo de las energías y configuraciones geométricas del estado fundamental y del primer estado excitado de dichas moléculas, la representación de las curvas de energía potencial (PECs, por sus siglas en inglés) y las densidades electrónicas.
Aunque el tema puede ser asociado a la química cuántica y computacional, las moléculas consideradas, en especial los iones, son de interés astrofísico.
La molécula más simple, el catión trihidrógeno H_3^+ está presente en las atmósferas de Júpiter, Urano y Saturno y también en las nubes interestelares densas y difusas. Su observación permite determinar, entre otros, la tasa de ionización de los rayos cósmicos o el tamaño de una nube.
Al igual queö el ión positivo, se sospecha que el H_3^- podría estar presente en el medio interestelar contribuyendo a bandas de absorción.
La molécula neutra H_3 se incluye para completar el estudio de sistemas con tres centros y dos (H_3^+), tres (H_3) y cuatro (H_3^-) electrones.
El primer paso consiste en una serie de cálculos que sólo requieren números atómicos y constantes, que se llaman cálculos *ab initio* (latín para *a partir de primeros principios*). Se empieza con el método Hartree-Fock (HF) de campo autoconsistente para resolver la ecuación de Schrödinger independiente del tiempo. Inicialmente, se aplica la aproximación de Born-Oppenheimer para desacoplar el movimiento de los electrones y núcleos con el fin de obtener la ecuación de Schrödinger puramente electrónica. Además, se define la función de onda en forma de una determinante de Slater, construida por espín-orbitales que se forman mediante combinaciones lineales de orbitales atómicos. El método HF aplica el principio variacional para encontrar los coeficientes correspondientes a los espín-orbitales que minimizan la energía. En práctica, se realiza un proceso iterativo puesto que las ecuaciones dependen de su solución.
El método HF promedia la interacción entre los electrones del sistema, lo cual significa que no considera interacciones instantáneas. Además, no tiene en cuenta la correlación electrónica, aparte del canje electrónico. Con el objetivo de incluir dicha correlación electrónica y por consiguiente, mejorar los resultados, se han desarrollado otros métodos, llamados post-HF. Los métodos empleados en esta tesis son la teoría perturbativa de Møller–Plesset (MPPT) y el método Coupled Cluster (CC). Aunque MPPT y CC utilizan procedimientos distintos, su forma de incluir la correlación electrónica es a través de combinaciones de determinantes de Slater del estado fundamental y de estados excitados.
Dado que el método HF trabaja con una combinación lineal de orbitales atómicos, una

elección de una base de funciones que describen los orbitales. Varias familias de conjuntos de bases existen, combinando en la mayoría de los casos funciones gaussianas contraídas para aproximar la forma real de los orbitales. La base elegida en esta tesis es la aug-cc-pVQZ desarrollada por Dunning. Esta base es optimizada para los métodos que contienen la correlación electrónica y solamente trata los electrones de valencia. Además incluye orbitales de momento angular mayor para añadir más flexibilidad a la hora de aproximar enlaces o electrones débilmente ligados.
El último paso práctico consiste en la aplicación del modelo semi-empírico de Hückel, el cual comienza, similar al método HF, con el principio variacional y la definición de la función de onda como combinación lineal de orbitales atómicos. El desarrollo lleva a la ecuación secular que permite encontrar los valores de la energía y los coeficientes de la combinación lineal. Para resolver dicha ecuación, el modelo utiliza un Hamiltoniano simplificado e introduce parámetros experimentales, lo cual fundamenta el carácter semi-empírico. Con la ayuda de los resultados *ab initio* los parámetros han sido determinados y la veracidad de los suposiciones del modelo ha sido comprobada.
Los cálculos *ab initio* HF-SCF, MPPT y CC se realizaron con el paquete de software de código abierto NWChem accesible a través del nodo 41 contenido en el cluster del departamento de física. Para iniciar un cálculo, se tiene que escribir un fichero de entrada, incluyendo información sobre el sistema, en este caso la geometría molecular inicial, el grupo de simetría y la carga. Además, se elige la base y el método deseado, cuyos detalles pueden ser ajustados, como por ejemplo el número máximo de iteraciones.
Antes de estudiar las moléculas principales de este trabajo, se ha calculado con los diferentes métodos la energía y, si procede, la longitud de enlace de las especies sospechadas de ser productos de la disociación de las moléculas. En este paso previo, gracias a los valores de la literatura, ya se puede prever una jerarquía de los métodos con respecto a su exactitud.
En el caso del $H_3{}^+$ se obtiene que, en el estado fundamental, la molécula forma un triangulo equilátero y en el primer estado excitado, la configuración es lineal simétrico. Los resultados de la energía de equilibrio son consistentes con los valores de la literatura. Sus canales de disociación son por un lado, dos átomos de hidrógeno y un protón, tanto en el estado fundamental como en el estado excitado, y por otro lado una molécula H_2 más un protón en el estado fundamental y una molécula $H_2{}^+$ más un átomo de hidrógeno en el estado excitado.
Se ha encontrado que en configuración triangular la molécula H_3 es inestable en su estado fundamental. En el estado excitado, la curva de potencial presenta un mínimo, pero debido a la exactitud limitada del cálculo, no se puede resolver ese mínimo con certeza. En ambos casos, el canal de disociación consiste en tres átomos de hidrógeno.
Por último, el $H_3{}^-$ es estable en una configuración lineal asimétrica, tanto en el estado

fundamental como en el estado excitado. Las energías y longitudes de enlace encontradas son compatibles con los valores de la literatura. Uno de los canales de disociación es una molécula H_2 más un ión de hidrógeno. Otro canal, una molécula H_2^- más un átomo de hidrógeno se puede intuir a partir de las mapas de densidad obtenidas con el modelo de Hückel.
Para mejorar los resultados, se propone la ampliación de las PEC a otras configuraciones, especialmente en el caso de la molécula neutra.

1 Introduction

1.1 Historical Facts and Astrophysical Motivation

The following information is taken from the articles [1] [2] [3], unless other reference is given.

The present thesis is centered on the electronic and geometric structure of the molecules H_3^+, H_3 and H_3^-. Even though this project can be assigned to the field of Quantum Chemistry or Molecular Physics, the studied molecule ions hold a high level of interest in Astrophysics.
The trihydrogen cation H_3^+ is the simplest polyatomic molecule and known to be the most abundant one in space next to H_2. In 1911 it was discovered by J. J. Thomson as radiation in a discharge tube with a mass to charge ratio three times greater than the one of H^+. The principal formation reaction $H_2^+ + H_2 \longrightarrow H_3^+ + H$ was discovered by T. R. Hogness and E. G. Lunn. In 1961, the conclusion that H_3^+ exists in the interstellar medium was made. Given that the cation acts as a proton donor, it was held responsible for the accelerated formation of diverse molecules that have been detected previously.
Followed by the first detection in the laboratory by T. Oka, who predicted that the only spectral lines of H_3^+ are located in the IR region and caused by vibrational transitions, its emission spectrum was found in the planetary ionospheres of Jupiter, Uranus and Saturn. Interstellar H_3^+ was revealed by the detection of its absorption spectrum, on the one hand in the sight line of two young stars embedded in a dense cloud in 1996 and on the other hand in diffuse clouds toward the galactic center in 1997.
The formation of H_3^+ requires a previous ionization of H_2 by, for instance, cosmic rays. Its destruction process differs depending on the environment: in dense clouds the dominating mechanism is the proton transfer to CO and in diffuse clouds H_3^+ is mainly destroyed by dissociative recombination with an electron.
The number density in these two domains can be found by equating the formation and destruction rates. Besides, the observable column density is related to the path length and to the cosmic ray ionization rate ζ. Accordingly, either the corresponding cloud size or the ionization rate can be determined.
Other possible applications of H_3^+ are the exploitation as a cosmic thermometer or densitometer by measuring its emitted intensities[4].
The existence of a stable negative ion H_3^- was predicted by N. Bohr in 1919 and experimentally observed from discharge plasmas by Wang et al. in 2003[5]. Just like its

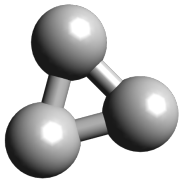

(A) Trihydrogen cation H_3^+.

(B) Trihydrogen anion H_3^-.

FIGURE 1.1: Ground state equilibrium configurations. The represented geometric configurations have been calculated in this work (see section 4).

positive counterpart, H_3^- is stable at the temperature of the interstellar medium. As other anionic hydrogen clusters, H_3^- is also suggested to exist in diffuse interstellar clouds, contributing to absorption bands[6].
When H_3^+ was discovered, it was thought to be the ionized version of a stable H_3 molecule. The existence of such a molecule was controversial for a long time and its history is marked by the back and forth of evidence and disproof. Since the detection of its spectral lines, also in a discharge tube by G. Herzberg[7], it is known that H_3 exists.
The triatomic hydrogen is considered to be an intermediate in the dissociative recombination process of H_3^+[8] and will be included in this project for completeness.

1.2 Objectives

By adding H_3 to the investigation, it becomes possible to study the electronic and geometric structure of a three center system and an increasing number of electrons: H_3^+ with two, H_3 with three and H_3^- with four electrons.
The simplest one, H_3^+, a closed shell molecule, forms an equilateral triangle in its electronic ground state (see Figure 1.1a), belonging to the D_{3h} symmetry group. The bonding arises from the delocalized electrons resulting in a resonant structure. In its first excited triplet state, it can exist in a linear symmetric shape.
Other than in its first excited state, the triatomic hydrogen H_3 is unstable in its ground state. To explore this molecule, an equilateral triangle configuration for both the ground and excited state is presumed.
The trihydrogen ion H_3^-, another closed shell molecule, presents in its ground state as well as in the first excited state a linear antisymmetric shape (see Figure 1.1b), belonging to the $C_{\infty v}$ symmetry group. The ion H_3^- is held together by a van der Waals anion induced dipole bonds.

The first step of the investigation consists of *ab initio* (latin for *from the beginning*) calculations provided by the computational chemistry software package NWChem. In this context, *ab initio* means that the methods employed to solve the Schrödinger equation only imply fundamental constants and atomic numbers. The Hartree-Fock self-consistent field (HF-SCF) method, is a first example for an *ab initio* calculation. It forms the foundation of more sophisticated methods, like the Møller–Plesset perturbation theory (MPPT) and the Coupled Cluster (CC) methods, pursuing the objective to improve the HF results by including electronic correlation. Therefore, these kind of methods are called post-HF.
In this thesis, the focus lies on calculations executed with the afore mentioned CC and MPPT methods, aiming to find the equilibrium energies and geometries of the molecules in their ground and first excited states. The results are compared to literature values, if available, to evaluate the accuracy of the methods employed.
Another interesting concept for the study of the molecules are potential energy surfaces (PES)[9]. In general, a PES describes the potential energy as a function of the geometry of a system, forming a complicated hypersurface of 3N-6[1] dimensions. They provide information about the optimal configuration, dissociation channels, equilibrium reaction constants and subsequently the present amount of a species. In case of the studies molecules, $N = 3$ so the PES depends on three degrees of freedom. There are several sets of coordinates adapted to the molecular species. One of them are the Jacobi coordinates: R, as the distance between two proton, ρ and θ, the modulus and orientation angle of the position vector of the third proton with respect to the center of mass between the other two protons. Another one is the distances between one selected proton of the molecule and the other two together with the angle between the corresponding position vectors. In this project coordinate sets are used but only the dependence on one coordinate is considered, resulting in potential energy curves (PECs) which are easier to handle than high dimensional PES. In practice the PECs are obtained fixing the orientational angle θ while varying the bond lengths between the atoms that constitute the molecule. The following two options have been chosen to perform this variation: on the one hand, the size of the molecules is reduced or increased as a whole, what means that all the bonds are increased by the same amount, and on the other hand the position of two atoms is held fixed while the third atom is approached or removed. With the curves on hand, the previously calculated equilibrium geometries are confirmed and possible dissociation channels are proposed.
The final step consists of a qualitative consideration, applying the semi-empirical Hückel molecular orbital (HMO) model, which works with empirical parameters and a simplified Hamiltonian operator. The results obtained involve the electronic ground and first

[1] In case of linear molecules the PES would have 3N-5 dimension

excited state and the associated wave functions of the systems. Using these wave functions, the electron density distribution is determined an represented graphically.

2 Theoretical Background

The following information is taken from the books [10] [9] [12] and [11], unless other reference is given.

2.1 Hartree-Fock (HF) self-consistent field (SCF) Method

The main problem of this work is to solve the time-independent Schrödinger equation in the most accurate way to obtain the electronic energy and wave function of the molecules under study. Instead of tackling the entire molecule, the Born-Oppenheimer (BO) approximation allows to decouple the electronic and nuclear motion by considering the atomic nuclei as point particles fixed in space. This approach leads to the electronic Schrödinger equation

$$(H_{el} + V_{NN})\Phi(\boldsymbol{r};\boldsymbol{R}) = E_{el}(\boldsymbol{R})\Phi(\boldsymbol{r};\boldsymbol{R}) \tag{2.1}$$

with the non-relativistic electronic Hamiltonian in atomic units [a.u.]

$$H_{el} = -\frac{1}{2}\sum_i \nabla_i^2 - \sum_{i,l}\frac{Z_l}{r_{il}} + \frac{1}{2}\sum_{i\neq j}\frac{1}{r_{ij}} \tag{2.2}$$

$$\Rightarrow \sum_i h_i + \frac{1}{2}\sum_{i\neq j} v_{ij}. \tag{2.3}$$

The first term of (2.2) corresponds to the kinetic energy of the electrons, the second term to the interaction between electron and nucleus and the third term to the electron-electron interaction. After the second equality sign, the single and pair contributions are summed up to simplify the notation, substituting

$$h_i = -\frac{1}{2}\nabla_i^2 - \frac{Z_l}{r_{il}} \tag{2.4}$$

and the electron-electron interaction

$$v_{ij} = \frac{1}{r_{ij}}. \tag{2.5}$$

The nucleus-nucleus repulsion term V_{NN} in (2.1) is a constant due to the BO approximation and will be neglected in the following[1]. Another consequence is the parametric dependence of the electronic energy and wave function on the nuclear locations, thus solving (2.1) for different positions $\boldsymbol{R}$ gives the potential energy surface (PES) whereof more information can be obtained.
If the electron-electron interaction in (2.3) is ignored for a moment, the Hamiltonian becomes separable and the total wavefunction can be written as a product of one-electron wavefunctions ϕ, the Hartree product

$$\Phi_{HP}(\boldsymbol{r_1}, ..., \boldsymbol{r_{N_e}}) = \phi_1(\boldsymbol{r_1}) \cdot ... \cdot \phi_{N_e}(\boldsymbol{r_{N_e}}) \tag{2.6}$$

with N_e number of the electrons. The main problem concerning this product is that the spin property is missing and does not satisfy the antisymmetry principle for fermions. By substituting the purely spatial functions $\phi_i(\boldsymbol{r_i})$ in (2.6) by orthonormal spin-orbitals $\chi(\boldsymbol{x})$, the spin property is taken into account. The four dimensional $\boldsymbol{x}$ includes the space and spin coordinates. Employing the Slater determinant in short notation for the total wavefunction

$$\Psi = (N_e!)^{-\frac{1}{2}} \det|\chi_1(\boldsymbol{x_1})\chi_2(\boldsymbol{x_2})...\chi_{N_e}(\boldsymbol{x_{N_e}})| \tag{2.7}$$

the antisymmetric character is given. The Slater determinant also respects the fact that electrons are indistinguishable and guarantees the fulfillment of the Pauli principle.
The electronic energy can be calculated by

$$E_{el} = \langle \Psi | H_{el} | \Psi \rangle \tag{2.8}$$

with H_{el} from (2.3), including the electron-electron term again. Evaluating (2.8) with the help of the Slater-Condon rules and slightly changing the notation yields

$$E_{HF} = \sum_{i}^{N_e} \langle i|h|i\rangle + \frac{1}{2}\sum_{i,j}^{N_e}[ii|jj] - [ij|ji] \tag{2.9}$$

with the one- and two-electron integrals defined as

$$\langle i|h|j\rangle = \int d\boldsymbol{x_1}\chi_i^*(\boldsymbol{x_1})h(\boldsymbol{r_1})\chi_j(\boldsymbol{x_1}) \tag{2.10}$$

$$[ij|kl] = \int d\boldsymbol{x_1}d\boldsymbol{x_2}\chi_i^*(\boldsymbol{x_1})\chi_j(\boldsymbol{x_1})\frac{1}{r_{12}}\chi_k^*(\boldsymbol{x_2})\chi_l(\boldsymbol{x_2}). \tag{2.11}$$

Here the subscripts 1 and 2 are introduced to illustrate the functionality of the one- and two-electron integrals. They are not related to the tags used in (2.7).

[1] Its only effect is the shifting of the eigenvalue and can be added at the end.

The Hartree-Fock method states that the spin-orbital which minimizes the energy (2.8) is the best approximation of the true one. Applying the variational theorem to (2.9), under the condition that the spin-orbitals remain orthonormal, leads to the Hartree-Fock equations

$$f(\boldsymbol{x_1})\chi_i(\boldsymbol{x_1}) = \epsilon_i\chi_i(\boldsymbol{x_1}) \tag{2.12}$$

with the energy ϵ_i corresponding to the spin-orbital i and the one-electron Fock operator

$$f(\boldsymbol{x_1}) = h(\boldsymbol{x_1}) + \sum_{j}^{N_e} J_j(\boldsymbol{x_1}) - K_j(\boldsymbol{x_1}) \tag{2.13}$$

where $J_j(\boldsymbol{x_1})$ is the Coulomb operator, giving the average potential at $\boldsymbol{x_1}$ produced by the charge distribution of the electron in orbital j. The exchange operator $K_j(\boldsymbol{x_1})$ is a mathematical consequence of the antisymmetry principle and can be understood as an interaction between electrons of the same spin. These two operators are defined as

$$J_j(\boldsymbol{x_1})\chi_i(\boldsymbol{x_1}) = \left[\int d\boldsymbol{x_2}|\chi_j(\boldsymbol{x_2})|^2\frac{1}{r_{12}}\right]\chi_i(\boldsymbol{x_1}) \tag{2.14}$$

$$K_j(\boldsymbol{x_1})\chi_i(\boldsymbol{x_1}) = \left[\int d\boldsymbol{x_2}\chi_j^*(\boldsymbol{x_2})\frac{1}{r_{12}}\chi_i(\boldsymbol{x_2})\right]\chi_j(\boldsymbol{x_1}). \tag{2.15}$$

Due to the fact that the Hartree-Fock equations (2.12) depend on their solutions $\chi_i(\boldsymbol{x_1})$, the best way to solve them is by numeric iteration, the self consistent field (SCF) procedure, where the spin-orbitals inserted to run a certain iteration step are the ones calculated in the previous step. These spin-orbitals χ_i are expressed as a linear combination of atomic orbitals (LCAO)

$$\chi_i = \sum_{\mu=1}^{N_o} C_{\mu i}\tilde{\chi}_\mu \tag{2.16}$$

where $\tilde{\chi}_\mu$ is a set of N_o atomic orbital basis functions which have to be chosen previously. Introducing (2.16) to (2.12), multiplying by $\tilde{\chi}_\mu^*$ on the left hand side and integrating gives the Hartree-Fock-Rothaan equations

$$\sum_\nu F_{\mu\nu}C_{\nu i} = \epsilon_i\sum_\nu S_{\mu\nu}C_{\nu i} \tag{2.17}$$

$$\Rightarrow \boldsymbol{FC} = \boldsymbol{SC\epsilon} \tag{2.18}$$

with the diagonal eigenvalue matrix $\boldsymbol{\epsilon}$, the coefficient vector $\boldsymbol{C}$, the overlap matrix $\boldsymbol{S}$ and the Fock matrix $\boldsymbol{F}$ described by the following expressions:

$$F_{\mu\nu} = \int d\boldsymbol{x_1} \tilde{\chi}^*_\mu(\boldsymbol{x_1}) f(\boldsymbol{x_1}) \tilde{\chi}_\nu(\boldsymbol{x_1}) \tag{2.19}$$

$$S_{\mu\nu} = \int d\boldsymbol{x_1} \tilde{\chi}^*_\mu(\boldsymbol{x_1}) \tilde{\chi}_\nu(\boldsymbol{x_1}). \tag{2.20}$$

If the basis set is chosen to be orthogonal, the overlap matrix is zero and (2.17) turns out to be a pure eigenvalue problem.
After the SCF procedure, the coefficients which constitute the best combination of spin-orbitals are identified. Hence the wavefunction (2.7) can be constructed and the total energy (2.9) can be determined.
To simplify the calculation of the integrals, different assumptions on the spin states can be made, such as the restricted (RHF) Hartree-Fock approach used for closed shell molecules, where all the electrons are constrained to be paired.

2.2 Post-Hartree-Fock Methods

One mayor downside of the HF-SCF method is that except for the exchange term (2.15), the interaction between the electrons is ignored. The Coulomb interaction is treated as a mean field effect instead of an instantaneous interaction. Therefore, a difference between the HF energy and the exact energy, the so called electronic correlation energy, exists.
However, the HF method provides a foundation for methods which aim to take electronic correlation into account. These methods are summed up by the term Post-Hartree-Fock, such as the Møller-Plesset Perturbation Theory or the Coupled Cluster method, discussed in the following.

2.2.1 Møller-Plesset second order perturbation theory (HF-MP2)

The objective of the Møller-Plesset (MP) method is to improve the Hartree-Fock results by estimating the correlation energy. To do so, the method makes use of perturbation theory.
It begins with stating that the electronic Hamiltonian H can be separated into an unperturbed part $H^{(0)}$ and a perturbation term $H^{(1)}$. The unperturbed part it chosen to be the sum of the Fock operators from (2.13)

$$H^{(0)} = H_{HF} = \sum_{i=1}^{N_e} f_i. \tag{2.21}$$

The perturbation operator $H^{(1)}$ then becomes

$$H^{(1)} = H - H_{HF} = \frac{1}{2}\sum_{i\neq j}\frac{1}{r_{ij}} - \sum_{ij} J_j(i) - K_j(i) \tag{2.22}$$

and can be seen as the deviation from the average interaction approach.
In perturbation theory, the first step consists of expanding the wavefunction and eigenvalue in powers of a parameter λ and inserting the expansion into the Schrödinger equation. Equating the the terms corresponding to the same order in λ, one obtains for the zeroth order

$$H^{(0)}\,|\Psi^{(0)}\rangle = E^{(0)}\,|\Psi^{(0)}\rangle \tag{2.23}$$

$$\Rightarrow H_{HF}\,|\Psi_{HF}\rangle = \sum_{i=1}^{N_e}\epsilon_i\,|\Psi_{HF}\rangle \tag{2.24}$$

thus the zeroth order energy is $\boldsymbol{E^{(0)} = \sum_{i=1}^{N_e}\epsilon_i}$. It is important to remember that if the spin-orbitals from (2.12) are eigenfunctions of the Fock operator, the ground state Slater determinant (2.7) (here called Ψ_{HF}) is an eigenfunction of H_{HF}.
The first order correction would be

$$E^{(1)} = \langle\Psi_{HF}|H^{(1)}|\Psi_{HF}\rangle \tag{2.25}$$

but rather than solving the integrals[2], the sum of $E^{(0)}$ and $E^{(1)}$ will be evaluated:

$$E^{(0)} + E^{(1)} = \langle\Psi_{HF}|H_{HF}|\Psi_{HF}\rangle + \langle\Psi_{HF}|H^{(1)}|\Psi_{HF}\rangle = \langle\Psi_{HF}|H|\Psi_{HF}\rangle = E_{HF}, \tag{2.26}$$

showing that the sum of zeroth and first order energy equal the total Hartree-Fock energy (2.9). The conclusion is that an actual correction to E_{HF} begins at higher orders.
Continuing with the second order correction, the associated expression is

$$E^{(2)} = \sum_{j>0}\frac{|\,\langle\Psi_j^{(0)}|H^{(1)}|\Psi_{HF}\rangle\,|^2}{E^{(0)} - E_j^{(0)}} \tag{2.27}$$

where $\Psi_j^{(0)}$ are the zeroth order excited Slater determinants. In accordance to the Brillouin's theorem, single excited Ψ_j will not contribute, that means only the double excited

[2]Solving the integrals, one finds that $E^{(1)}$ is the electron-electron interaction term with negative sign, the one that is counted twice in the sum of the orbital energies ϵ_i.

Ψ_j remain after applying the Slater-Condon rules, finally giving for (2.27)

$$E^{(2)} = \sum_{i}^{occ}\sum_{j>i}^{occ}\sum_{a}^{vir}\sum_{b>a}^{vir}\frac{([ij|ab] - [ij|ba])^2}{\epsilon_i + \epsilon_j - \epsilon_a - \epsilon_b} \tag{2.28}$$

with the two electron integrals defined in (2.11), the occupied orbitals i, j and unoccupied (virtual) orbitals a, b.
The final energy given by this method is

$$E_{MP2} = E^{(0)} + E^{(1)} + E^{(2)} = E_{HF} + E^{(2)}. \tag{2.29}$$

In this project, only second order (MP2) corrections will be used, but in general, higher order corrections are possible (MP3, MP4).

2.2.2 Coupled Cluster (CC)

The Coupled Cluster (CC) theory is another method for upgrading the Hartree-Fock results. It starts with the definition of its wavefunction which arises from a reference, in this case, the HF wavefunction

$$|\Psi_{CC}\rangle = e^T |\Psi_{HF}\rangle \tag{2.30}$$

where T is the cluster operator

$$T = T_1 + T_2 + ... + T_{N_e} \tag{2.31}$$

composed of the excitation operators T_i that create the i-electron excited Slater determinants when acting on Ψ_{HF}. For T_1 and T_2 the effect is described in the following way:

$$T_1 |\Psi_{HF}\rangle = \sum_{i}^{occ}\sum_{a}^{vir} t_i^a |\Psi_i^a\rangle \tag{2.32}$$

$$T_2 |\Psi_{HF}\rangle = \sum_{i<j}^{occ}\sum_{a<b}^{vir} t_{ij}^{ab} |\Psi_{ij}^{ab}\rangle . \tag{2.33}$$

The sub- and superscripts are defined as in (2.28), the wavefuntions $|\Psi_i^a\rangle$ and $|\Psi_{ij}^{ab}\rangle$ stand for one- and two-electron excited Slater determinants, respectively, and the coefficients t are called amplitudes.
Depending on the T_i included in (2.31), the method's name is abbreviated: CCS, CCSD, CCSDT (S→ singly, SD→ singly and doubly, SDT→ singly, doubly and triply excited).

Another form of the CCSDT method is the CCSD(T) where the triplet contribution is estimated by the use of perturbation theory, invoking terms obtained from MP4 and MP5[13].
Expanding the exponential from (2.30), inserting (2.31) and rearranging in groups of the same excitation yields

$$e^T = 1 + T_1 + \left(T_2 + \frac{1}{2}T_1^2\right) + \left(T_3 + T_2T_1 + \frac{1}{6}T_1^3\right) + ... \tag{2.34}$$

The first term reproduces the HF wavefunction, the second term creates all singly excited determinants, the third term creates all doubly excited determinants and so on.
After introducing the previous expansions into 2.30 the Coupled Cluster wavefuntion becomes

$$|\Psi_{CC}\rangle = |\Psi_{HF}\rangle + \sum_{ia} t_i^a |\Psi_i^a\rangle + \sum_{i<j}\sum_{a<b}(t_{ij}^{ab} + t_i^a t_j^b - t_i^b t_j^a)|\Psi_{ij}^{ab}\rangle + ... \tag{2.35}$$

The first term in parenthesis results from T_2, the so called connected double excitation, and the cross terms in parenthesis follow from $\frac{1}{2}T_1^2$, the disconnected double excitation.
To find the energy E_{CC}, the Schrödinger equation is projected against $|\Psi_{HF}\rangle$

$$\langle\Psi_{HF}|H|\Psi_{CC}\rangle = E_{CC}. \tag{2.36}$$

Using (2.35) together with Brillouin's theorem and the Slater-Condon rules, the final expression for the energy results in

$$E_{CC} = E_{HF} + \sum_{i<j}\sum_{a<b}([ij|ab] - [ij|ba])(t_{ij}^{ab} + t_i^a t_j^b - t_i^b t_j^a). \tag{2.37}$$

That means, as long as T_1 and T_2 are included the Coupled Cluster energy is always given by (2.37), due to the fact that higher excitations are eliminated.
Projecting the Schrödinger equation against excited determinants leads the equations for t_i^a, t_{ij}^{ab} and so on. The concrete form of these equations depends on the operator (2.31) chosen, but in general, they constitute a system of coupled equations which can only be solved iteratively.
In summary, MP2 as well as CC include electronic correlation by means of deviations from the single Slater determinant approach, since both methods create a mix of the ground and excited state Slater determinants.

2.3 Basis sets

As mentioned before, the *ab initio* methods require the selection of a basis set for the LCAO in equation (2.16).
The election of the functions should be reasonable in a chemical sense, that means the shape of atomic orbitals should be described correctly. Slater-type orbitals (STOs) satisfy this condition but mathematically, they are impracticle as the two-electron integrals in (2.11) cannot be solved analytically with STOs.
A solution to the problem is the use of Gaussian-type orbitals GTOs. In cartesian coordinates, the form of a GTO centered on an atomic nucleus is

$$g_{ijk}(\boldsymbol{r}) = Nx^i y^j z^k e^{-\alpha r^2} \tag{2.38}$$

with $\alpha > 0$, normalization constant N and positive integers i, j, k, defining the nature of the orbital described, for example $i = j = k = 0$ corresponds to s-type orbitals, $i + j + k = 1$ to p-type orbitals, where three different combinations are possible, leading to p_x, p_y and p_z orbitals.
Even though GTOs present computational advantages since they permit the calculation of the integrals, STOs reflect the correct orbital shape, especially around the nucleus. To approximate the STO shape, contracted Gaussians are used:

$$\chi_o = \sum_i d_{oi} g_i \tag{2.39}$$

where d_{oi} are the contraction coefficients and g_i the primitive Gaussians from (2.38). The coefficients as well as the exponents of the g_i are known from previous optimizations and remain fixed during the iteration process.
Several families of basis sets build their basis functions from contracted Gaussians whereupon the number of basis functions used for each orbital may vary. For instance, the minimal or single-ζ basis set, STO-nG uses one basis function for each orbital, constructed by n primitive Gaussians. Accordingly, multiple-ζ basis sets use more than one basis function. Another approach is the split-valence basis set by Pople. As the name implies, it consists of a distinction between core and valence orbitals, ascribing a different number of functions to each of them.
The basis set family employed in this project is the correlation consistent ('cc') polarized ('p') valence-only ('V') basis set designed by Dunning[14] with the full notation cc-pVXZ, where 'X' stands for the number of functions ζ, adopting the letters D,T,Q,.. (double, triple, quadruple,..). Correlation consistent means that the coefficients and exponents have been optimized for calculations which include electron correlation. The fact that the basis set is polarized implies that functions of higher angular momentum

are present to add more flexibility suitable for describing molecular bonds[3]. In the case of first row atoms (H and He), the structure of orbitals obeys the following scheme:

- cc-pV**D**Z uses **two** s orbitals for the valence 1s orbital and adds one set of p orbitals for polarization
- cc-pV**T**Z uses **three** s orbitals for the valence orbital and adds two sets of p orbitals and one set of d orbitals
- cc-pV**Q**Z uses **four** s orbitals for the valence orbital and adds three sets of p orbitals, two set of d orbitals and one set of f orbitals.

Besides polarization functions, diffuse Gaussians with small exponents can be added to model the function shape far from the nucleus in order to provide flexibility for weakly bound electrons like in anions. In practice, diffuse functions are included in the basis set by adding an extra function for each angular momentum present, resulting in the 'augmented' basis set aug-cc-pVXZ.
Once a basis set is chosen, the respective coefficients and exponents of the contracted Gaussians (2.39) can be found in the Exchange Basis Set repository[15].
The ideal case of a basis set is the use of an infinite number of functions, the complete basis set (CBS), but in practice, only finite basis sets can be implemented, unless extrapolation techniques are used to reach the CBS limit. The finite character implies the appearance of a truncation error. To minimize this error and achieve a high accuracy, one could think about using a large basis set. However, it is important to be aware of the fact that a high number of basis functions results in a higher computational cost so that a compromise has to be made.

2.4 Hückel Molecular Orbital (HMO) Model

Apart from the *ab initio* calculations, the species under question are also studied with the semi-empirical Hückel method. The objective is to find the energy level structure, the corresponding wave functions and following to that, the electron density of the molecular electronic state.
Similar to the HF method, the Hückel theory is based on the variational principle aiming to minimize the energy of the system by varying the wavefunction. The general expression for the energy in (2.8) is

$$\frac{\int \Psi H \Psi d\boldsymbol{r}}{\int \Psi^2 d\boldsymbol{r}} \geq E_0, \tag{2.40}$$

[3]The basis set for a hydrogen atom would consist of s orbitals. However, combining only s orbitals for the hydrogen molecule is not sufficient to describe the H-H bond properly so a set of p orbitals has to be added.

which always figures an upper bond for the energy. Substituting the wavefunction Ψ by a LCAO of the form

$$\Psi = \sum_{i}^{N} a_i \varphi_i, \tag{2.41}$$

where the a_i are the variational coefficient and φ_i represent the atomic orbitals associated with the N atoms. Taking the derivative of the energy to find the minimum, one obtains a system of N equation

$$\sum_{i=1}^{N} a_i (H_{ki} - E S_{ik}) = 0 \qquad \forall k \tag{2.42}$$

where H_{ki} is the matrix element $\langle \varphi_k | H | \varphi_i \rangle$ called resonance integral, and S_{ik} is the overlap matrix as in (2.20)

$$S_{ik} = \int \varphi_i \varphi_k d\boldsymbol{r}. \tag{2.43}$$

Only if the determinant formed by $(H_{ki} - E S_{ik})$ is equal to zero, equation (2.42) has a non-trivial solution. The expression where the determinant is set to be zero is called secular equation and yields to solutions for the energy E. The coefficients a_i can than be determined by substituting the energies into (2.42) and solving the system of equations obtained for each solution of E. In this procedure, it is important to remember that the wavefunctions have to be orthogonal and normalized.
In order to simplify the computation of (2.42), the HMO assumes the following conventions[10]:

1. $S_{ik} = \delta_{ik}$, meaning that the atomic orbitals do not overlap
2. $H_{ii} = \alpha$, fixing the same energy value for each atom
3. $H_{ik} = \beta_{ik}$ only if the atoms i and k are direct neighbors, otherwise $H_{ik} = 0$.

The experimental parameters α and β are defined to be negative[9]. Item 2. and 3. show the semi-empirical character of the HMO, since they reflect the simplification of the Hamiltonian.
Actually, the HMO was developed for planar hydrocarbon π-electron systems, that means the atomic orbitals are supposed to be of the type p. For the σ-electron systems studies in this project, this constraint is ignored, and one s-type orbital per atom, centered on the nucleus, is assigned. From this follows that N in (2.42) is equal to the number of atoms.
The assumption that $H_{ii} = \alpha$ only holds for high symmetry molecules, such as those with equilateral triangle shape. Nevertheless, it is adopted for the linear configurations as well.

Furthermore, the approximation of zero overlap is questionable. Thus, S is included and determined in the calculations to evaluate the validity of the assumption.
Once the coefficients a_i have been found, the total wavefunction associated with the energy levels can be composed and the electron density can be estimated.

3 NWChem Software

For the *ab initio* calculations, the open source computational chemistry software package NWChem developed by the Experimental Molecular Science Laboratory (EMSL) at the Pacific Northwest National Laboratory (PNNL)[16] was employed. The tools provided in this package enable, among others, quantum mechanical calculations such as SCF-HF, post-HF and Density Functional Theory (DFT). Furthermore, it is possible to treat large systems and their dynamics, to include relativistic effects and to study excited states.
The program is accessible on the node 41 of the computer cluster Molec3 in the Department of Physics of the University of La Laguna.
In order to launch a calculation, an input file must be set up. It includes a series of commands to define the system and to configure the chosen method. In the following list, some of the most important commands for this project are specified[17]:

- START[1] + *name*: initiating and assigning a name to the job and to the associated auxiliary files created during calculation
- ECHO: Print the input file at the beginning of the output file
- GEOMETRY + *input units*: List of atoms followed by their cartesian coordinates
  - SYMMETRY: Point group of the molecular geometry
- BASIS: Fixing the basis set for every atom. The basis functions are taken from the basis set library included in NWChem
- CHARGE: Charge of the ion
- SCF: Self-consistent field HF calculation. Even if post-HF methods are performed, the underlying HF calculation is executed previously. Some possible specifications are:
  - UHF/RHF/ROHF: Unrestricted, Restricted or Restricted Open shell HF
  - SINGLET/DOUBLET/TRIPLET: Multiplicity of the energy state
  - NOPEN: Number of singly occupied orbitals (open shells)

[1] Previous to this directive, a memory allocation command can be added.

  - MAXITER: Maximum number of iterations, occasionally needed to facilitate convergence

- TCE (*Tensor Contracted Engine*): A module consisting of programs interfaced with NWChem implementing approximations to optimize the calculations. Some methods, like the combination of MP2 and ROHF or the CCSDT are only possible when embedded in the TCE module. One of the optimizations used in TCE is:

  - DIIS (*Direct Inversion in the Iterative Subspace*): Extrapolation procedure to reduce the number of iterations and stabilize convergence. Indicating a value, for example DIIS 10 means that the procedure is performed every ten iterations

- TASK + *method* + *task*: To select the method and the calculation task. Possible methods are SCF, MP2, CCSD(T) and CCSDT, when included in the TCE. The task *Optimize* determines the lowest energy and by varying the geometry. Task *Energy* is used to obtain potential energy curves since it fixes the configuration and calculates the associated energy

Other constraints, such as the convergence threshold, are set to default. A sample input file is provided in appendix A.
To finally launch the calculation, a one-line command in the node prompt is necessary, providing the number of processors and the names of the input and output file.

4 Results and Discussion

The following calculations have been realized using exclusively the **aug-cc-pVQZ** basis set, including 46 functions (5s4p3d2f) for hydrogen, which are contracted Gaussians consisting of a varying number of primitives. This choice was made after some trial calculations, testing possible candidates and showing that the aug-cc-pVQZ basis set yields to the most accurate results. In addition, it is also used in similar contexts in the literature.

Before analyzing the results for $H_3{}^+$, H_3 and $H_3{}^-$, their possible dissociation products are presented. Table 4.1 includes the optimized equilibrium ground state energies calculated with HF, MP2, CCSD(T) and CCSDT and the corresponding bond lengths, in the case of molecular hydrogen and its positive ion. For closed shell systems, such as H_2 and later $H_3{}^+$, the CCSD(T) was used and for open shell systems, the CCSDT method. It was verified[1] that the two methods do not differ in a relevant extent, so that both CCSD(T) and CCSDT are denoted CCSD(T) in the following.

TABLE 4.1: Ground state equilibrium energies and bond lengths (in [a.u.]) of the possible asymptotic dissociation species calculated with HF, MP2 and CCSD(T)

	H_2 $(X^1\Sigma_g^+)$	$H_2{}^+$ $(X^2\Sigma_g^+)$	H^- (^1S)	H (^2S)
HF	-1.133532	-0.602554	-0.487827	-0.499953
MP2	-1.166853	-0.602554	-0.517153	-0.499953
CCSD(T)	-1.173907	-0.602554	-0.527162	-0.499953
Literature	-1.174719[18]	-0.602635[18]	-0.527634[19]	-0.500000
MP2 bond length	1.39	2.00		
CCSD(T) bond length	1.40	2.00		
Literature[18]	1.40	2.00		

It can be seen that the bond length literature values are well reproduced by the CCSD(T) method, while MP2 shows a slight deviation in the third decimal in case of H_2. Considering the energy results, a hierarchy of the methods becomes visible: for one-electron systems, HF gives the same value as MP2 and CCSD(T) because electron correlation does not occur. For systems with more than one electron the post-HF methods are superior to HF in terms of accuracy. The best results with an accordance up to the third decimal are provided by CCSD(T).

[1] As an example, the energy of the $H_3{}^+$ ground state calculated with CCSD(T) is $E = -1.343233$ a.u. while with CCSDT the energy is $E = -1.343238$ a.u.. The difference lies in the sixth decimal, irrelevant for the comparison with literature values conducted in this section.

4.1 Trihydrogen cation H_3^+

4.1.1 Electronic Structure and Potential Energy Curves (PECs)

The singlet ground state and first excited triplet state equilibrium geometries, calculated with CCSD(T) and the corresponding energies of H_3^+, calculated with MP2 and CCSD(T) are summarized in table 4.2.
In the ground state, H_3^+ is a stable molecule in the form of an equilateral triangle, belonging to the point group D_{3h}, with side length $R^e = 1.65$ a.u. and in the first excited triplet state, it takes a linear symmetric shape, with an internuclear distance of 2.45 a.u. These results are in agreement with the literature.
Similar to the dissociation species, the best energy results for H_3^+ originate from the CCSD(T) calculations, with an accuracy up to the third decimal in both energy states.

TABLE 4.2: H_3^+ ground $^1A_1'$ and first excited $^3\Sigma_u^+$ state equilibrium energies and geometric configurations calculated with MP2 and CCSD(T) (energies and distances in [a.u.]).

	Bond length	MP2 Energy	CCSD(T) Energy
$^1A_1'$ (equilateral triangle)	$R^e = 1.65$	-1.335840	-1.343231
Literature	$R^e = 1.65$[18]	-1.343837[18]; -1.343836[20]	
$^3\Sigma_u^+$ (linear symmetric)	$R^e_{ab} = 2.45$ $R^e_{bc} = 2.45$ $R^e_{ac} = 4.91$	-1.115135	-1.115989
Literature[21]	$R^e_{ab} = 2.45$ $R^e_{bc} = 2.45$ $R^e_{ac} = 4.90$	-1.116046	

Different than in optimization jobs, potential energy curves (PECs) are obtained by fixing the position of the protons and calculating the associated energy, where each point of the curve belongs to a different position. Comparing the asymptotic energies with combinations of the energy values of the species from table 4.1, the dissociation products can be identified.
Due to the accuracy of the CCSD(T) results in table 4.1 and 4.2, the PECs are calculated exclusively with the CCSD(T) method.

Figure 4.1 shows the PECs of the H_3^+ ground state. In Figure 4.1a the potential energy is presented as a function of the triangle size R. The minimum of the curve at $R = 1.65$ a.u. confirms the result obtained from geometry optimization. At high values for R, the molecule dissociates into two free hydrogen atoms and a free proton. Another information that can be drawn from 4.1a is the full dissociation energy as the difference between the asymptotic energy and the minimum of the curve. For H_3^+, the full dissociation energy is $E_{dis} = 0.343231$ a.u.

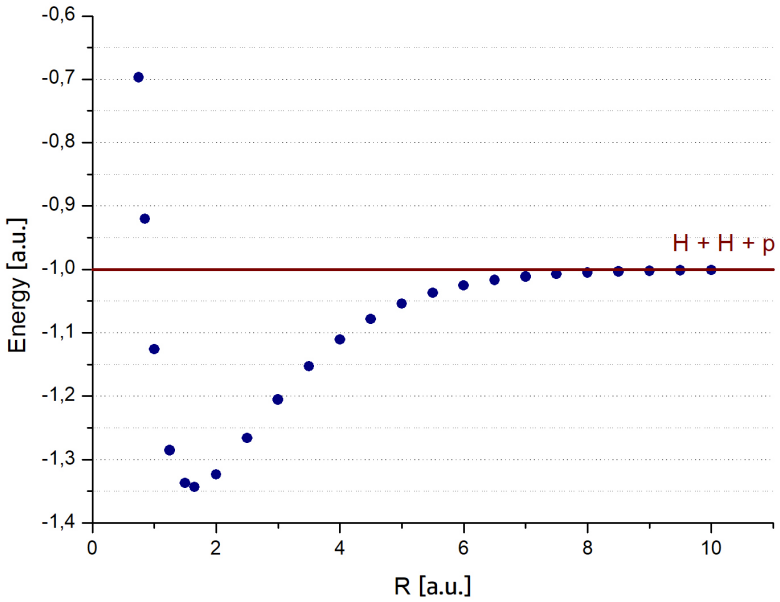

(A) Potential energy curve associated to the ground state as a function of the triangle size R calculated with CCSD(T). The asymptotic limit corresponds to a dissociation into two free hydrogen atoms and a free proton. The horizontal line is drawn at the literature value taken from Table 4.1.

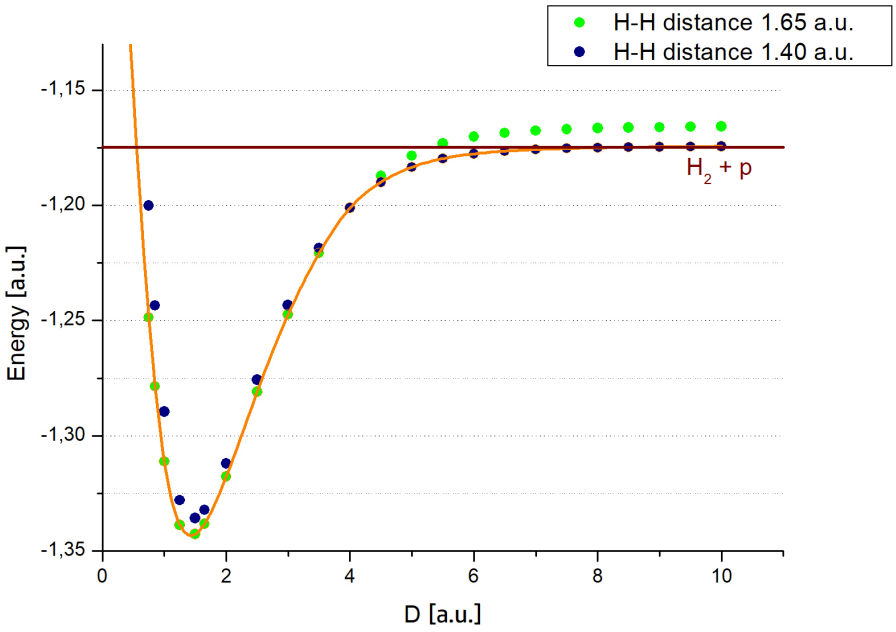

(B) Potential energy curve associated to the ground state as a function of the distance D between the center of mass of two fixed hydrogen atoms (H-H) and a proton, which is removed from the molecule. The (H-H) distance is fixed at the H_3^+ (green) and H_2 (blue) ground state equilibrium. The asymptotic limit corresponds to a dissociation into a free H_2 and a free proton. The horizontal line is drawn at the literature value taken from Table 4.1.

FIGURE 4.1: H_3^+ ground state potential energy curves.

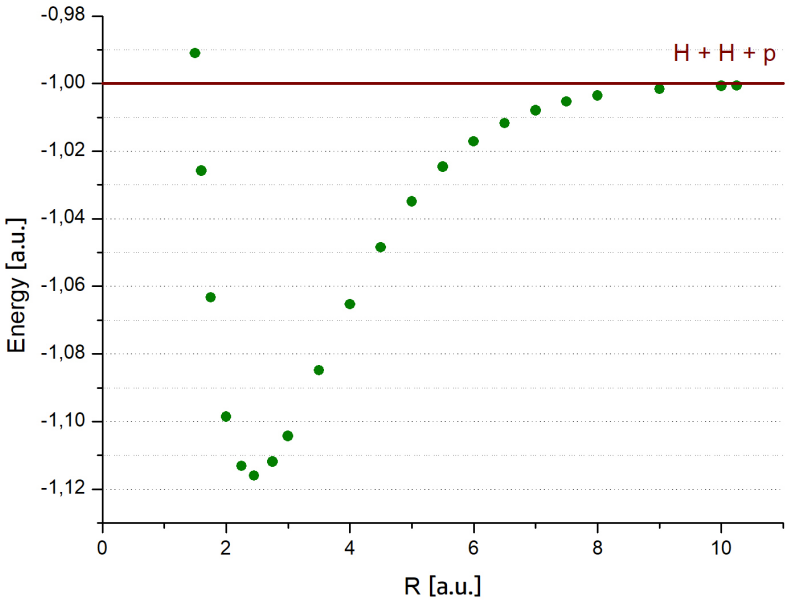

(A) Potential energy curve associated to the ground state as a function of the size $R = R_{ab} = R_{bc}$ calculated with CCSD(T). The asymptotic limit corresponds to a dissociation into two free hydrogen atoms and a free proton. The horizontal line is drawn at the literature value taken from Table 4.1.

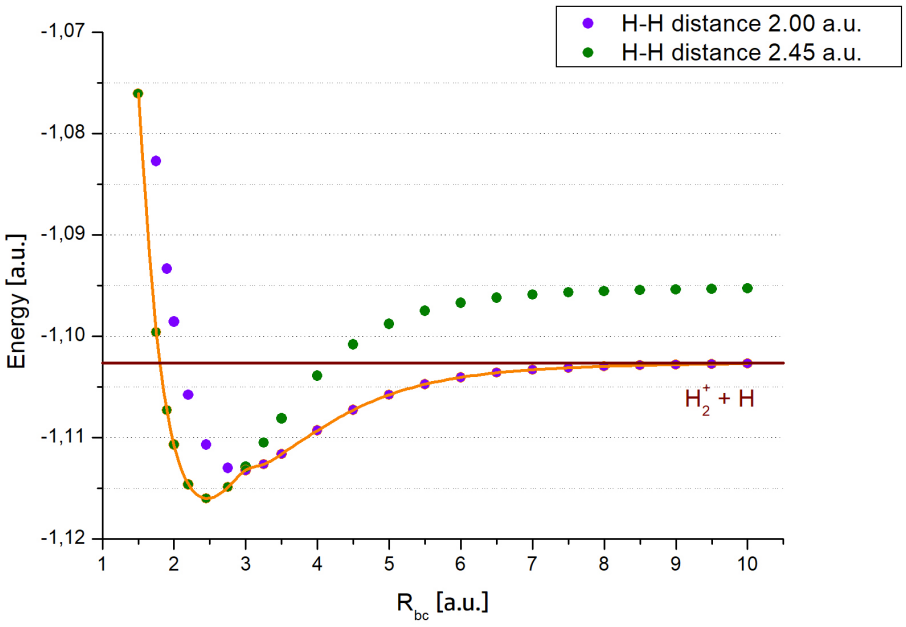

(B) Potential energy curve associated to the ground state as a function of the distance $R = R_{bc}$ between two fixed hydrogen atoms (H-H) and a proton, which is removed from the molecule. The (H-H) distance is fixed at the H_3^+ excited state (green) and H_2 ground state (violet) equilibrium. The asymptotic limit corresponds to a dissociation into a free H_2^+ a free hydrogen atom. The horizontal line is drawn at the literature value taken from Table 4.1.

FIGURE 4.2: H_3^+ first excited triplet state potential energy curves.

The second ground state PEC in figure 4.1b represents the behavior of the molecule when one proton is removed. To obtain the green curve, two of the three H atoms are fixed on the y-axis at the $H_3{}^+$ ground state equilibrium distance between them, while their center of mass lies in the origin. In other words, one side of the triangle stays unaltered. The third H atom varies its distance D on the x-axis, approaching or removing itself from the center of mass of the two fixed H atoms, maintaining an isoceles triangular configuration. For the blue curve, the procedure is repeated, fixing the distance between the two H atoms on the y-axis at the H_2 ground state equilibrium.
For small distances, the configuration with a distance of 1.65 a.u. between the two H atoms possesses a lower energy, because at $R = 1.65$ a.u. it passes through the equilateral equilibrium configuration of $H_3{}^+$. At higher distances, when the atom is far from the remaining hydrogen molecule, the curves cross and the equilibrium configuration of H_2 presents a lower energy than a H_2 with a bond length of $R = 1.65$ a.u. This fact indicates that the dissociation products are a free H_2 and a free proton.
A better illustration of this transition could be achieved performing a geometry optimization on the H_2 for each point. Instead of two curves, only one would be needed for this case.
For the excited state, the PECs are obtained in the same way. Firstly, in figure 4.2a, the whole molecule in linear configuration is dispersed, increasing the the distance of both bonds $R_{ab} = R_{bc}$. Again, the minimum confirms the optimization result. The asymptotic limit shows that in the excited state the molecule dissociates into the same products as the ground state, with a dissociation energy of $E_{dis} = 0.115989$ a.u.
The PECs in figure 4.2b are obtained by fixing the distance between two of the hydrogens on the x-axis equal to the bond length of a $H_2{}^+$ molecule for the purple curve and equal to $R^e_{ab} = 2.45$ a.u. (table 4.2) for the green curve and approaching or removing the third H atom, also along the x-axis. Now the transition between the two configurations takes place shortly after the passage through the equilibrium of the excited $H_3{}^+$. The abruptness of the transition can be assigned to the difference between the slopes of the curves in this point. A geometry optimization in each step, as suggested before, may give rise to a smoother curve.
The purple curve has a lower energy in the asymptotic region, indicating that the $H_3{}^+$ molecule in its first excited state dissociates into a free $H_2{}^+$ a free hydrogen atom.

4.1.2 Application of the HMO Model

In order to start applying the HMO method to the equilateral triangle configuration of $H_3{}^+$, the reference system has to be established. Its origin is defined by the center of mass of the triangle. The x-axis, which also figures one of the C_2 symmetry axis of the

system, passes through one of the protons and the z-axis coincides with the C_3 symmetry axis. Besides, the protons occupying the vertices of the triangle are named a, b, c and the atomic orbitals from (2.41) centered on the respective protons are called $1s_a, 1s_b$ and $1s_c$, since only one s-type orbital for each atom is used.
The secular equation arising from (2.42) after adopting the Hückel conditions is then given by

$$\begin{vmatrix} \alpha-\epsilon & \beta-S\epsilon & \beta-S\epsilon \\ \beta-S\epsilon & \alpha-\epsilon & \beta-S\epsilon \\ \beta-S\epsilon & \beta-S\epsilon & \alpha-\epsilon \end{vmatrix} = 0. \tag{4.1}$$

Due to symmetry, the overlap integrals S and the parameters β are set to be equal ($S = S_{ab} = S_{bc} = S_{ac}$; $\beta = \beta_{ab} = \beta_{bc} = \beta_{ac}$).
Evaluating (4.1) and recollecting that $\alpha, \beta < 0$, the lowest energy level is found to be

$$\epsilon_1 = \frac{\alpha + 2\beta}{1 + 2S} \tag{4.2}$$

with its corresponding wavefunction calculated with Mathematica

$$\Psi_1 = \frac{1}{\sqrt{3(1+2S)}}(1s_a + 1s_b + 1s_c). \tag{4.3}$$

The first excited level is two fold degenerate, without considering electronic spin, with an energy value of

$$\epsilon_2 = \epsilon_3 = \frac{\alpha - \beta}{1 - S} \tag{4.4}$$

and orthonormal wavefunctions

$$\Psi_2^{(1)} = \frac{1}{\sqrt{2(1-S)}}(-1s_a + 1s_c) \quad ; \quad \Psi_2^{(2)} = \frac{1}{\sqrt{2(1-S)}}(-1s_a + 1s_b). \tag{4.5}$$

It has to be kept in mind that the ground and excited states obtained with the HMO theory are based on the same geometry. Therefore, the ground state obtained from the HMO theory can be assigned to the $^1A_1'$ state from table 4.2 and the first excited state corresponds to a $^3E'$ state instead of a $^3A'$ state.
Knowing the mono electronic energy levels, the electron configuration can be established (see figure 4.3): in the ground state, two electrons occupy the ϵ_1 level and in the first excited state, one electron is located in ϵ_1 and the other one in the $\epsilon_2 = \epsilon_3$ level.

The total equilibrium energy of these states is assembled as follows:

$$E(^1A_1') = 2\epsilon_1 \tag{4.6}$$

$$E(^3E') = \epsilon_1 + \epsilon_2. \tag{4.7}$$

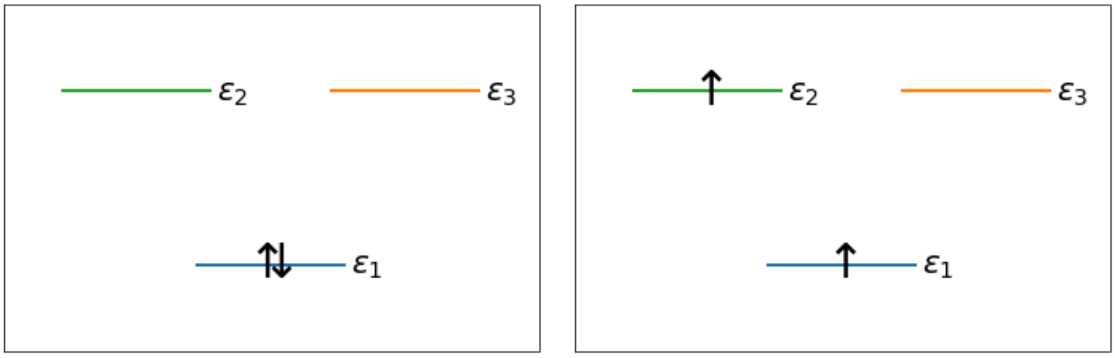

(A) Ground state configuration (B) One possible excited state configuration

FIGURE 4.3: Qualitative illustration of the H_3^+ ground and excited state mono electron configuration.

Their values have been determined using the same methodology in the reference [22]: $E(^1A_1') = -1.342520\,\text{a.u.}$[2] and $E(^3E') = -0.792082\,\text{a.u.}$. Substituting (4.2) and (4.4) into (4.6) and (4.7) and solving the system of equations, the parameters α and β are found to adopt the following values: $\alpha \simeq -0.538421\,\text{a.u.}$ and $\beta \simeq -0.494683\,\text{a.u.}$

Electron density

To continue the simple HMO analysis, the exact 1s wavefunction of hydrogen[23] in atomic units

$$\Psi_{1s}(r) = \frac{1}{\sqrt{\pi}} e^{-r} \tag{4.8}$$

where $r(x,y,z)$ denotes the absolute value of the position vector $\boldsymbol{r}(x,y,z)$, is chosen for the $1s_a, 1s_b$ and $1s_c$ atomic orbitals. Shifting the orbitals (4.8) to the positions of the protons and using (2.43), the off-diagonal elements of the overlap matrix can be evaluated numerically using Python, giving the result that $S = S_{ab} = S_{bc} = S_{ac} \simeq 0.683$ and therefore confirming the assumptions that the overlap is the same for every atom and $S \neq 0$.

[2]This result is slightly higher than the literature values and the CCSD(T) result from table 4.2, however, due to consistency reasons, $E(^1A_1')$ and $E(^3E')$ should originate from the same calculation procedure.

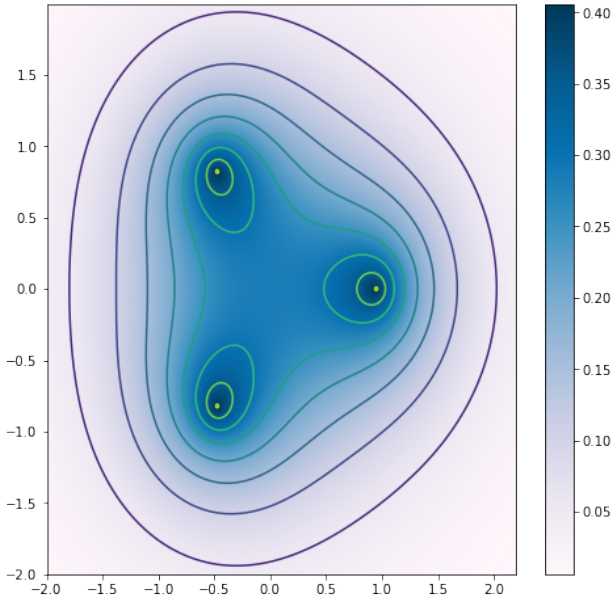

FIGURE 4.4: H_3^+ ground state density map $\rho(x, y, 0)$ obtained with the HMO model.

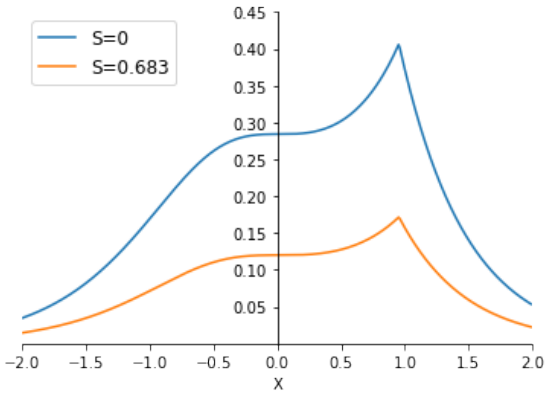

(A) Profile $\rho(x, 0, 0)$ in $[\text{a.u.}]^{-1}$ along the x-axis in [a.u.]

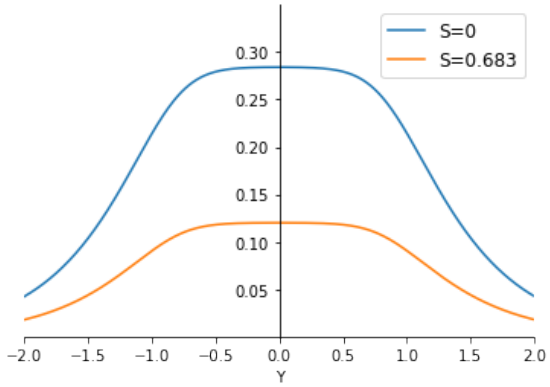

(B) Profile $\rho(0, y, 0)$ in $[\text{a.u.}]^{-1}$ along the y-axis in [a.u.]

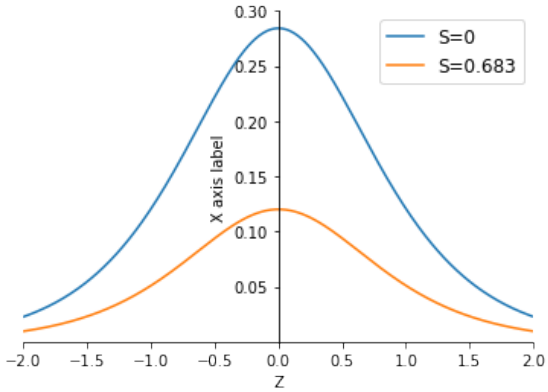

(C) Profile $\rho(0, 0, z)$ in $[\text{a.u.}]^{-1}$ along the z-axis in [a.u.]

FIGURE 4.5: H_3^+ ground state density profiles

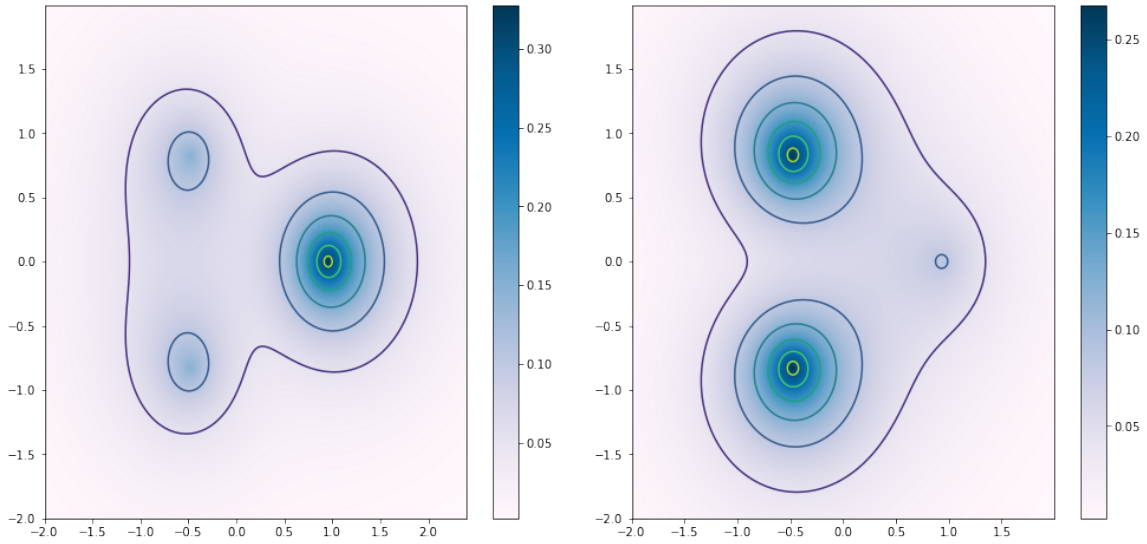

(A) Density map $\rho^+(x,y,0)$ (B) Density map $\rho^-(x,y,0)$

FIGURE 4.6: H_3^+ first excited state density maps obtained with the HMO model.

In the case of the ground state $^1A_1'$, the electron density can be estimated by

$$\rho(x,y,z) = 2|\Psi_1|^2. \tag{4.9}$$

Figure 4.4 shows the density map in the molecular plane $\rho(x,y,0)$ for the case with $S = 0.683$. The iso-density curves are drawn in steps of $0.05\,\text{a.u.}^{-1}$, in accordance with the color bar. It can be seen that the highest electron density is located around the protons. However, a charge density unequal to zero exists in the central region of the triangle, illustrating the delocalization of the electron.
In figure 4.5 the density profiles along the three spatial axis are represented for the cases $S = 0.683$ and $S = 0$. When no overlap is considered, the density is higher, since S appears in the denominator of (4.3) and (4.5).
In the first excited state $^3E'$, two combinations of Hückel's molecular orbitals (4.5) have to be considered in order to form the wavefunction Ψ_2 associated with the degenerate energy level:

$$\Psi_2^+ = \frac{1}{\sqrt{6(1-S)}}(\Psi_2^{(1)} + \Psi_2^{(2)}) \qquad \text{and} \qquad \Psi_2^- = \frac{1}{\sqrt{2(1-S)}}(\Psi_2^{(1)} - \Psi_2^{(2)}) \tag{4.10}$$

giving rise to two possible electron densities

$$\rho^+(x,y,z) = |\Psi_1|^2 + |\Psi_2^+|^2 \tag{4.11}$$
$$\rho^-(x,y,z) = |\Psi_1|^2 + |\Psi_2^-|^2 \tag{4.12}$$

which are represented in the molecular plane in figure 4.6. The electron density results,

both for the ground and excited state are compatible with the supplementary material reported in reference [20].

4.2 Trihydrogen H_3

4.2.1 Electronic Structure and Potential Energy Curves (PECs)

The neutral molecule H_3 can exist in different geometric configurations[24]. In the following, only the equilateral triangle shape will be considered for the ground (^2E) and the first excited state (^4E).

TABLE 4.3: H_3 gound ^2E and first excited ^4E state equilibrium energies and geometric configurations calculated with CCSD(T) (energies and distances in [a.u.]).

	Bond length	CCSD(T) Energy
^2E (equilateral triangle)	$R^e = 1.97$	-1.574747
^4E (equilateral triangle)	$R^e = 7.77$	-1.499915

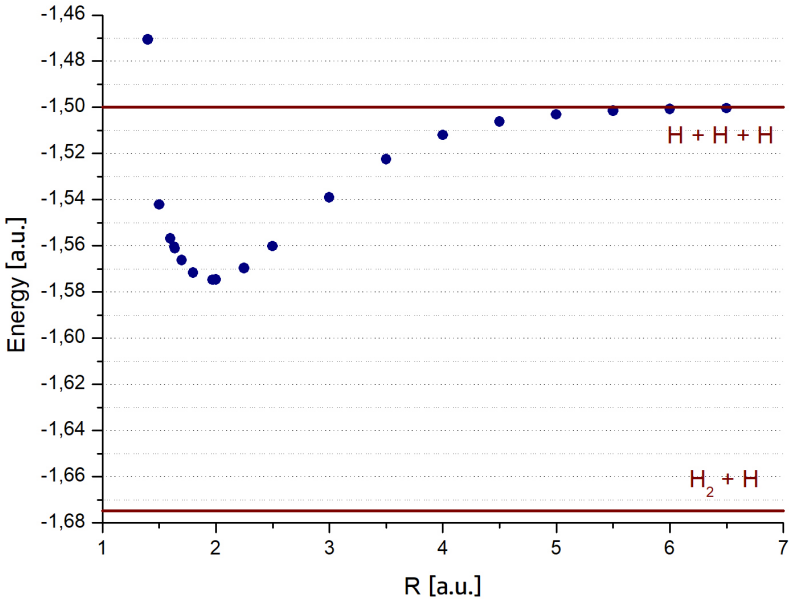

FIGURE 4.7: H_3 ground state energy as a function of the triangle size R calculated with CCSD(T). The asymptotic limit corresponds to a dissociation into three free hydrogen atoms. The second limit corresponds to the dissociation into one free hydrogen molecule and one free hydrogen atom and is included to prove the instability of the neutral molecule. The horizontal lines are drawn at the literature value taken from Table 4.1.

Table 4.3 summarizes the equilibrium energies and bond lengths. The ground state configuration presented does not originate from an optimization. The reason why the ground state is not presented in its optimized configuration lies in the peculiarity of this state to be influenced by the Jahn-Teller effect. Instead, it was determined by means of the PEC in figure 4.7, which shows a minimum at $R^e = 1.97$ a.u. and $E = -1.574747$ a.u. This value lies above the dissociation limit into one hydrogen molecule plus one hydrogen atom, calculated with the data shown in table 4.1. Accordingly, the neutral molecule cannot be stable in its ground state. Furthermore, the PEC indicates the possible dissociation into three free hydrogen atoms for high values of R, with a dissociation energy of $E_{dis} = 0.074747$ a.u.

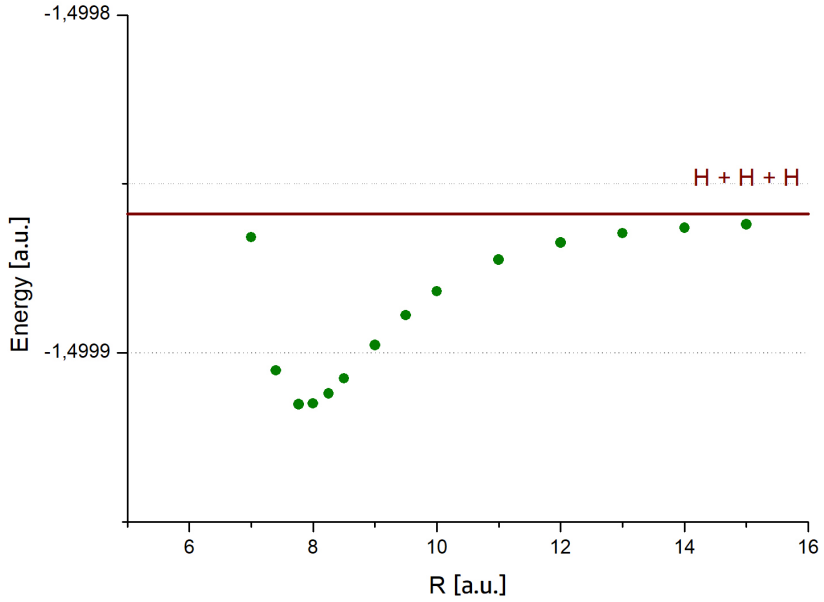

FIGURE 4.8: H_3 first excited quartet state energy as a function of the triangle size R calculated with CCSD(T). The asymptotic limit corresponds to a dissociation into three hydrogen atoms. The horizontal line is drawn at the literature value taken from Table 4.1.

In the case of the first excited state, the configuration was optimized using CCSD(T). The minimum is only observable after performing a zoom, as illustrated in figure 4.8. Because of consistency, the horizontal line is drawn at the calculated value from 4.1, given that the y-axis is strongly amplified and the error connected to the CCSD(T) becomes perceivable. The dissociation channel found for the excited state of H_3 also corresponds to three free hydrogen atoms.
Knowing from the results in table 4.2 that the accuracy of the CCSD(T) method is guaranteed up to the third decimal and obtaining that the minimum energy of H_3 and the

dissociation limit differ in the fourth decimal, the consequence is that the minimum cannot be detected with certainty. In other words, it is not possible to resolve the dissociation energy of $E_{dis} = 8.5 \cdot 10^{-5}$ a.u. with the employed calculation method. Due to that, no additional PECs for the search of dissociation channels have been calculated.

4.2.2 Application of the HMO Model

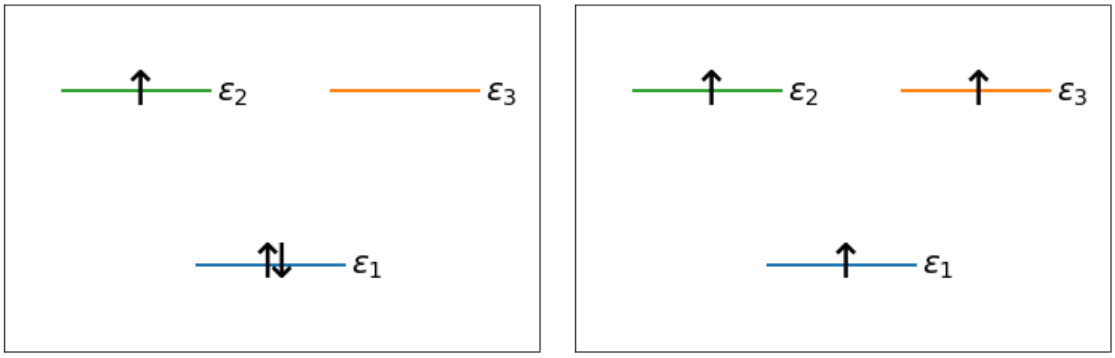

(A) One possible ground state configuration (B) First excited state configuration

FIGURE 4.9: Qualitative illustration of the H_3 ground and excited state mono electron configuration.

Since the configuration assumed for H_3 is the same as for H_3^+, the derivation of the energies and wavefunctions is the same as the one seen in section 4.1.2, the results corresponding to H_3 are equal to the equations (4.2)-(4.5). The only difference lies in the bond lengths, which have to be adopted to the values from table 4.3, and in the electronic configuration. Being a system of three electrons, two of them occupy the lowest energy level ϵ_1 forming a pair and one unpaired electron is located in the $\epsilon_2 = \epsilon_3$ level (see figure 4.9a). As for the first excited state of H_3^+, the ground state of H_3 presents two possible electron densities ρ^+ and ρ^-, displayed in figure 4.10a and 4.10b. Shifting the $1s$ wavefunctions to the positions of the atoms, the overlap was determined to be $S = 0.594$. The residual charge density in the central region of the H_3 is lower compared to H_3^+, what might be related to the instability of the H_3 molecule.
Concerning the first excited state, one of the two electrons in ϵ_1 migrates into the $\epsilon_2 = \epsilon_3$ level, but without forming a pair with the other electron located on this level (see figure 4.9b). The corresponding density map is presented in figure 4.10c, where the overlap was determined to be $S = 0.0122$.
The parameters α and β are obtained using the same procedure as in the case of H_3^+.

Now the total energies are compounded in the following way:

$$E(^2E) = 2\epsilon_1 + \epsilon_2 \tag{4.13}$$

$$E(^4E) = \epsilon_1 + 2\epsilon_2. \tag{4.14}$$

With the expressions (4.2) and (4.4), one obtains

$$E(^2E) = 2\frac{\alpha + 2\beta}{1 + 2S} + \frac{\alpha - \beta}{1 - S} \tag{4.15}$$

$$E(^4E) = \frac{\alpha + 2\beta}{1 + 2S'} + 2\frac{\alpha - \beta}{1 - S'}. \tag{4.16}$$

Substituting the energy values from table 4.1 and taking $S = 0.594$ and $S' = 0$, what is approximately true for the excited state, the parameters are $\alpha \simeq -0.499972$ a.u. and $\beta \simeq -0.179119$ a.u.

Although no PECs to explore other dissociation channels, such as those where one H atom is removed, have been calculated, the electron density map of the first excited state in figure 4.10c may give an evidence for an additional dissociation channel. It can be seen that the charge located around the atom on the x-axis is slightly higher than around the other two atoms. This could indicate a possible dissociation into a $H_2{}^+$ molecule and a H^-, when the geometric configuration is more appropriate.

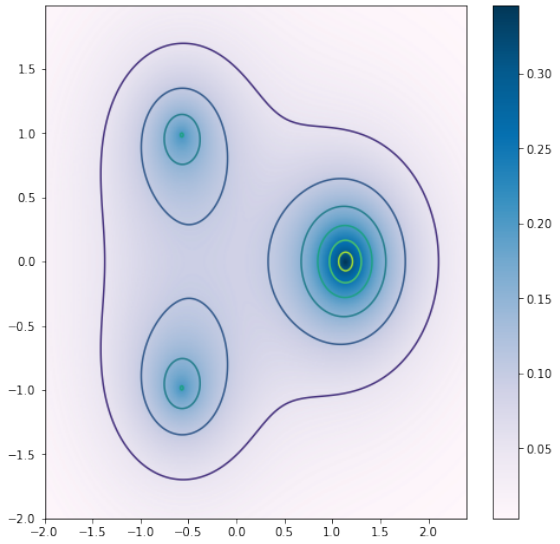

(A) Ground state density map $\rho^{+}(x, y, 0)$

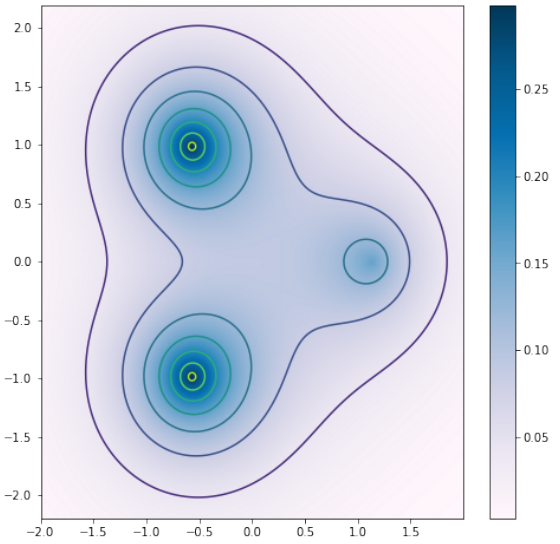

(B) Ground state density map $\rho^{-}(x, y, 0)$

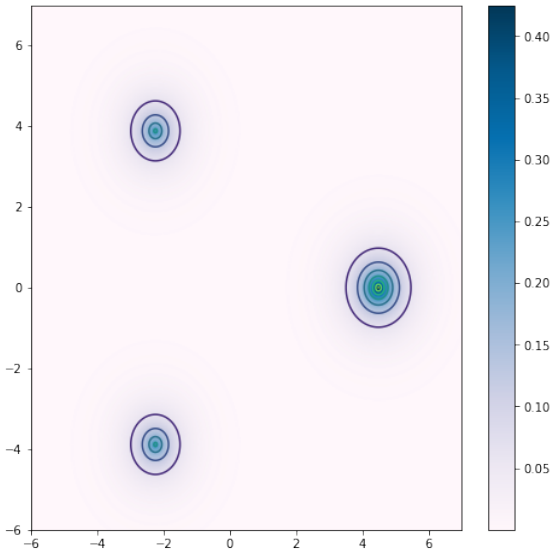

(C) First excited state density map

FIGURE 4.10: H_3 ground and first excited state density maps obtained with the HMO model.

4.3 Trihydrogen anion H_3^-

4.3.1 Electronic Structure and Potential Energy Curves (PECs)

Finally, the system with the highest number of electrons in this study, H_3^- will be analyzed. Table 4.4 summarizes the equilibrium configurations and energy values obtained from the *ab initio* optimizations.
The calculations reveal that the ground as well as the excited state exist in a linear asymmetric configuration. For the ground state, the results are in agreement with the literature values. Once again, the energy result is accurate up to the third decimal.
In the case of the first excited state only one references has been found, supporting the possibility of a linear asymmetric shape[25].
The distance R^e_{ab} attracts attention, since for both states it is equal or nearly equal to the equilibrium bond length of H_2.

TABLE 4.4: H_3^- ground $^1\Sigma$ and first excited state $^3\Sigma$ energies, calculated with MP2 and CCSD(T) and equilibrium geometries, calculated with CCSD(T). Energies and bond lengths in [a.u.].

	Bond length	MP2 Energy	CCSD(T) Energy
$^1\Sigma$ (linear asymmetric)	$R^e_{ab} = 1.41$ $R^e_{bc} = 5.57$ $R^e_{ac} = 6.99$	-1.686202	-1.702901
Literature[19]	$R^e_{ab} = 1.41$ $R^e_{bc} = 5.57$ $R^e_{ac} = 6.99$	-1.703298[19]	
$^3\Sigma$ (linear asymmetric)	$R^e_{ab} = 1.40$ $R^e_{bc} = 14.34$ $R^e_{ac} = 15.74$	-1.631235	-1.638646

The ground state potential energy as a function of the distance R_{bc} is shown in figure 4.11. In other words, one atom is removed from the molecule, maintaining the linear shape. The minimum of the curve coincides with the optimization results and the asymptotic limit indicates a dissociation into a free H_2 and a free H^-. For the horizontal line, the calculated energy values of the dissociation products from table 4.1 have been used, due to the same reason as in the case of 4.8. The small distance between the points and the line can be explained by the fact that the distance between the remaining H_2 is not exactly the same as the equilibrium distance of a hydrogen molecule.
Comparing the energies of the asymptotic line and the minimum of the curve, the full dissociation energy is found to be $E_{dis} = 1.832 \cdot 10^{-3}$ a.u.

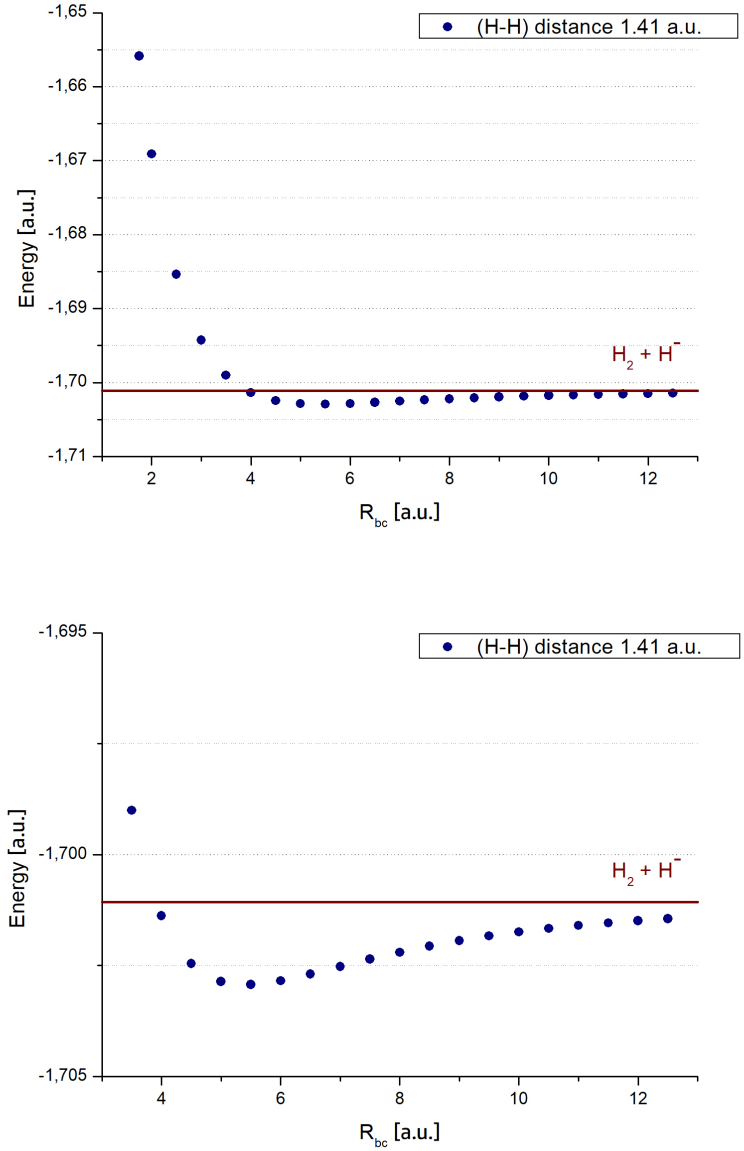

FIGURE 4.11: H_3^- ground state potential energy as a function of the distance R_{bc} calculated with CCSD(T). The (H-H) distance is fixed at the H_3^- equilibrium. Total curve (top) and amplification (bottom). The asymptotic limit corresponds to a dissociation into one free hydrogen molecule and one free hydrogen anion. The horizontal line is drawn at the calculated value taken from Table 4.1.

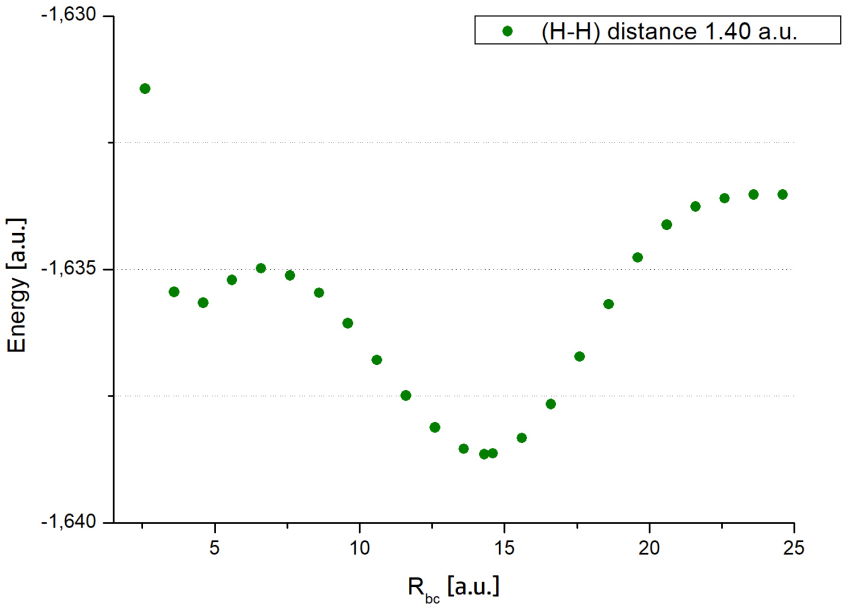

FIGURE 4.12: H_3^- first excited state energy as a function of the distance R_{bc} calculated with CCSD(T). The (H-H) distance is fixed at the H_3^- equilibrium.

In figure 4.12, the PEC of the excited state as a function of R_{bc} is presented. The global minimum confirms the result of 4.4. Combinations of the energies from table 4.1 do not lead to the identification of a definite dissociation channel. The inclusion of H_2^- was tested, yielding to an energy near -1.630 a.u. for the sum of a H_2^- molecule and a H atom. However, this value is also relatively far from the asymptotic region. In addition, no reference for the energy of a H_2^- molecule was found and therefore, it is not included in table 4.1.

A secondary minimum exists near $R_{bc} \approx 5$ a.u. It was verified, by the calculation of the potential energy as a function of R_{ab} fixing the distance R_{bc} at the value in this secondary minimum (see figure 4.13), that it also appears in the dimension of R_{ab}. In practice, with 4.12 and 4.13 two cuts of the two dimensional PES have been obtained. It can be concluded, that the secondary minimum corresponds to either a local minimum or a saddle point on the PES. To identify the definite character, a PEC as a function of the angle has to be added.

The dissociation energies are estimated by comparing the energy of the point at $R_{bc} \approx 25$ a.u. with the global minimum energy, finding that $E_{dis}^{(1)} = -0.069374$ a.u. and for the secondary minimum, comparing its energy with the local maximum near $R_{bc} \approx 7$ a.u., resulting in $E_{dis}^{(2)} = -1.588 \cdot 10^{-3}$ a.u.

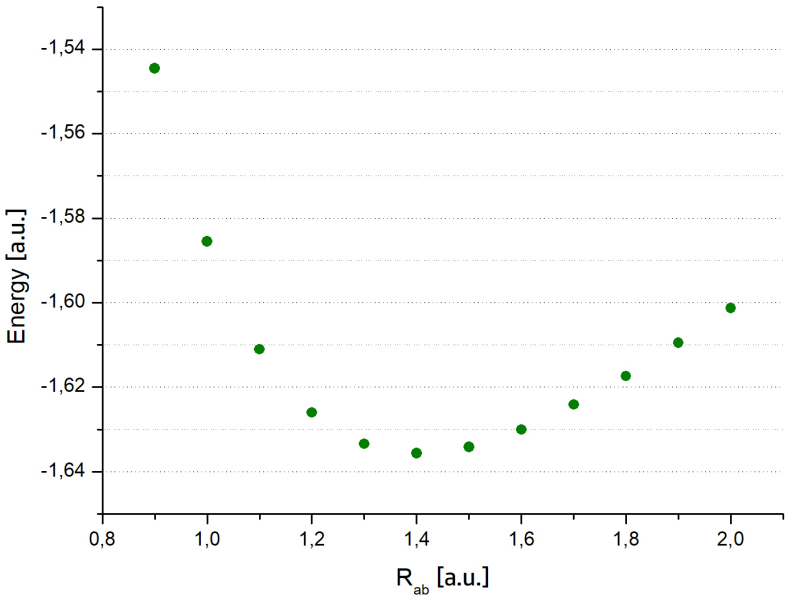

FIGURE 4.13: H_3^- first excited state energy as a function of the distance R_{ab} calculated with CCSD(T). The R_{bc} distance is fixed at the distance where the secondary minimum appears.

4.3.2 Application of the HMO Model

In the case of H_3^-, the *ab initio* calculations revealed a linear equilibrium configuration in the ground state. Hence, for the reference system it is suitable to align the molecule with the x-axis, fixing the proton named a in the origin, the proton b in $x = 1.41$ a.u. and proton c in $x = 5.57$ a.u., according to table 4.4. Consequently, there are only two pairs of direct neighbors: ab and bc. Due to the very different distance between these pairs, it is suggested to work with two parameters for the resonance integral, $\beta_{ab} = \beta_1$, $\beta_{bc} = \beta_2$ and taking $\beta_{ac} = 0$. In the same way, the overlap integral is expected to be zero for large distances, so that $S_{ac} = S_{bc} = 0$ and $S_{ab} = S$.
Adopting these constraints, the secular equation takes the following form:

$$\begin{vmatrix} \alpha - \epsilon & \beta_1 - S\epsilon & \beta_2 \\ \beta_1 - S\epsilon & \alpha - \epsilon & 0 \\ \beta_2 & 0 & \alpha - \epsilon \end{vmatrix} = 0. \tag{4.17}$$

Evaluating the determinant, the lowest energy level is

$$\epsilon_1 = \frac{1}{1 - S^2}(\alpha - \beta_1 S - \sqrt{\Delta}) \tag{4.18}$$

where Δ stands for

$$\Delta = (\alpha S - \beta_1)^2 + \beta_2^2(1 - S^2). \tag{4.19}$$

The wavefunction belonging to E_1 is than given by

$$\begin{aligned}\Psi_1 = &\frac{1}{(2(\beta_1 - S\epsilon_1)^2 + 2\beta_2^2 + 2(\beta_1 - S\epsilon_1)S\sqrt{(\beta_1 - S\epsilon_1)^2 + \beta_2^2})^{\frac{1}{2}}} \cdot \\ &\cdot \left(\sqrt{(\beta_1 - S\epsilon_1)^2 + \beta_2^2}1s_a + (\beta_1 - S\epsilon_1)1s_b + \beta_2 1s_c\right).\end{aligned} \tag{4.20}$$

The excited levels, this time not degenerate, are

$$\epsilon_2 = \alpha \tag{4.21}$$

with its wavefunction

$$\Psi_2 = \frac{1}{((\beta_1 - S\epsilon_2)^2 + \beta_2^2)^{\frac{1}{2}}}(\beta_2 1s_b + (\beta_1 - S\epsilon_2)1s_c) \tag{4.22}$$

and

$$\epsilon_3 = \frac{1}{1 - S^2}(\alpha - \beta_1 S + \sqrt{\Delta}) \tag{4.23}$$

with

$$\begin{aligned}\Psi_3 = &\frac{1}{(2(\beta_1 - S\epsilon_3)^2 + 2\beta_2^2 + 2(\beta_1 - S\epsilon_3)S\sqrt{(\beta_1 - S\epsilon_3)^2 + \beta_2^2})^{\frac{1}{2}}} \cdot \\ &\cdot \left(-\sqrt{(\beta_1 - S\epsilon_3)^2 + \beta_2^2}1s_a + (\beta_1 - S\epsilon_3)1s_b + \beta_2 1s_c\right).\end{aligned} \tag{4.24}$$

Electron density

Being a molecule with four electrons, in the ground state of $H_3{}^-$, two electrons occupy the ϵ_1 and the other two occupy the ϵ_2 level (see figure 4.14a). In the first excited state, one of the electrons in ϵ_2 migrates to the ϵ_3 level, forming a triplet state (see figure 4.14b).

Knowing the electron configuration, the density associated to the ground state represented in figure 4.15a can be calculated by means of

$$\rho(x, y, z) = 2|\Psi_1|^2 + 2|\Psi_2|^2. \tag{4.25}$$

For the graphic representation it was necessary to choose values for α, β_1 and β_2, given that the wavefunctions depend on these parameters. The selection is arbitrary, choosing $\alpha = -0.5$ a.u., $\beta_1 = -0.1$ a.u. and $\beta_2 = \frac{R_{ab}^e}{R_{bc}^e}\beta_1$, setting β_2 to be proportional β_1, weighted

(A) Ground state configuration (B) First excited state configuration

FIGURE 4.14: Qualitative illustration of the H_3^- ground and excited state mono electron configuration.

by the quotient $\frac{R^e_{ab}}{R^e_{bc}}$. Due to this approximation, the values of the parameters have not been calculated explicitly as done for H_3 and H_3^+.
The overlap integrals have been determined to be $S_{ab} = 0.75$, $S_{ac} = 0.06$ and $S_{bc} = 0.17$, confirming that the highest overlap occurs between the atoms a and b.
Figures 4.15b and 4.15c show profiles of the density map 4.15a along the x- and z-axis, manifesting that in the ground state, the charge is concentrated on atom c. This observation is in accordance with the dissociation channel found before in 4.11.
The figures also help to clarify the small deviation of the R^e_{ac} distance from the H_2 equilibrium. The presence of atom c with accumulated charge density provokes a small perturbation of the bond leading to a H_2 bond length of 1.41 a.u. instead of 1.40 a.u.

To find the electron density associated with the first excited state of H_3^-, the distances have to be adopted to the excited state configuration from table 4.4. The overlap integrals are in this case $S_{ab} = 0.75$, $S_{ac} = 4.96 \cdot 10^{-5}$ and $S_{bc} = 0.00017$, confirming even more the election of $S_{ac} = S_{bc} = 0$ than in the ground state. Considering the electron configuration from figure 4.14b, the density can be obtained by

$$\rho(x, y, z) = 2|\Psi_1|^2 + |\Psi_2|^2 + |\Psi_3|^2. \tag{4.26}$$

Choosing the same values for the parameters as in the ground state, the corresponding density is represented in figure 4.16a. Together with the density profiles along the x- and z-axis in figures 4.16b and 4.16c it becomes clear that in the first excited state, the charge distribution shifts towards the H_2 molecule. This fact might be an evidence for the existence of a H_2^++H dissociation channel.

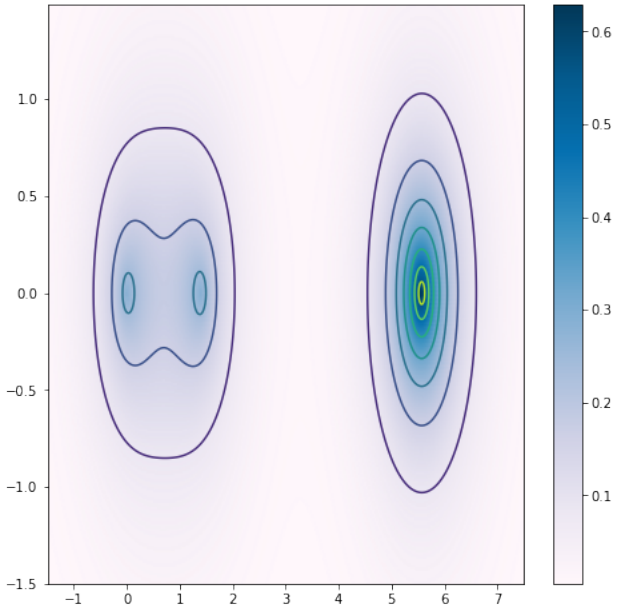

(A) H_3^- ground state density map $\rho(x, y, 0)$ obtained with the HMO model.

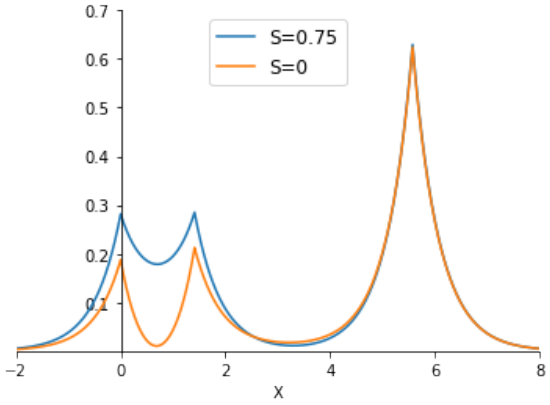

(B) Profile $\rho(x, 0, 0)$ in $[\text{a.u.}]^{-1}$ along the x-axis in [a.u.]

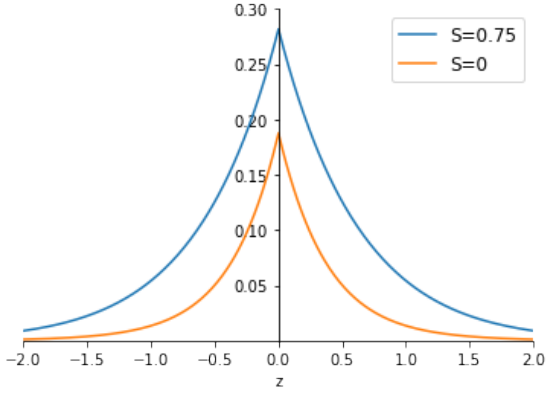

(C) Profile $\rho(0, 0, z)$ in $[\text{a.u.}]^{-1}$ along the z-axis in [a.u.]

FIGURE 4.15: H_3^- ground state density map and profiles. Due to symmetry, the profile along the y-axis is identical to the one along the z-axis.

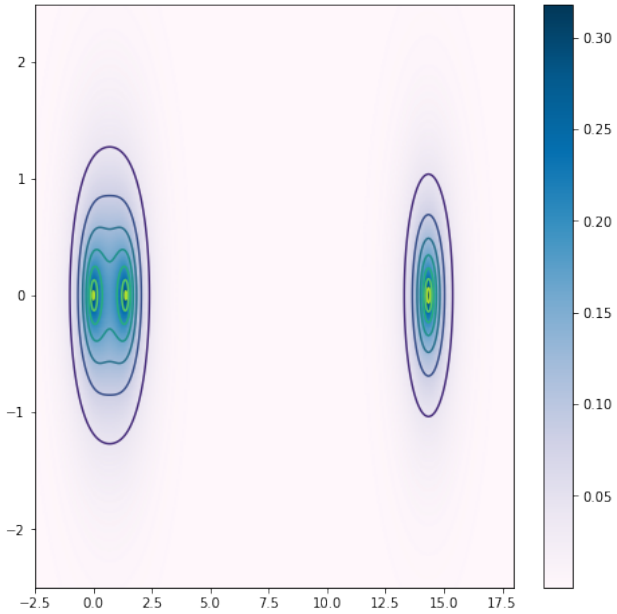

(A) H_3^- first excited state density map $\rho(x, y, 0)$ obtained with the HMO model.

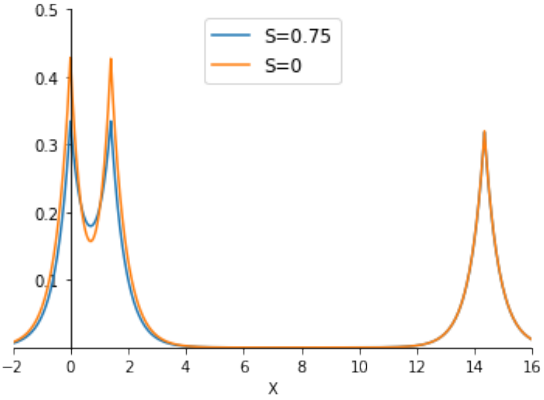

(B) Profile $\rho(x, 0, 0)$ in $[\text{a.u.}]^{-1}$ along the x-axis in [a.u.]

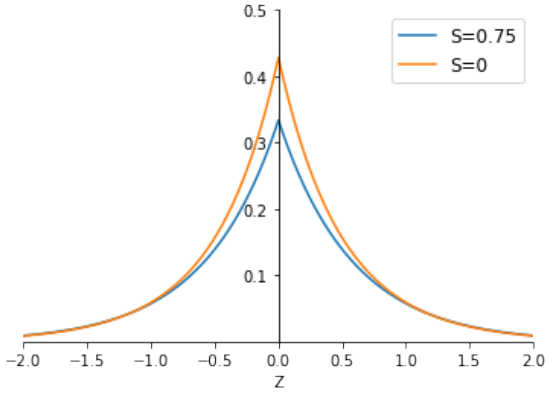

(C) Profile $\rho(0, 0, z)$ in $[\text{a.u.}]^{-1}$ along the z-axis in [a.u.]

FIGURE 4.16: H_3^- first excited state density map and profiles. Due to symmetry, the profile along the y-axis is identical to the one along the z-axis.

5 Conclusions

Comparing the performance of the methods, table 4.1 already gives an impression on the quality differences between HF, MP2 and CCSD(T) and their dependence on the size of the system. For example, the importance of electron correlation becomes clear when the number of electrons increases and the post-HF methods outmatch the simple HF calculation.
In summary, all the results obtained for the trihydrogen cation H_3^+ are in good agreement with the literature.
The results from table 4.2 allow the evaluation of the employed methods, finding that the CCSD(T) method in combination with the aug-cc-pVQZ basis set is accurate up to the third decimal. Given that the CCSD(T) method is the "gold standard" [9], an improvement could be achieved by choosing a larger basis set like the aug-cc-pV6Z used in the reference [18].
As mentioned before, a better way to calculate the PECs 4.1b and 4.2b might be a geometry optimization between the H_2 molecule in every step while the third H atom is removed progressively. It has to be inquired if NWChem provides a suitable way to realize this idea.
The case of the neutral molecule H_3 gives room for improvements, regarding the PECs and the accuracy of the numeric results. Knowing from the reference [24] that the excited states of H_3 can exist in various geometric configurations, such as linear symmetric and asymmetric, an exploration of these configurations could be realized if the accuracy of the calculation is increased. The article [24] also asserts that the energy levels of H_3 present degeneration and conical intersections, which are crossing of PECs corresponding to different states with the same symmetry. Thus, the level of complexity rises for the PECs of H_3 and a detailed analysis of this system could figure the topic of an advanced study.
The ground state energy as well as its geometry of the trihydrogen anion H_3^- are in accordance with the literature values. For the missing dissociation channel in figure 4.12 no solution is found so far. A general suggestion for both ground and excited state is the calculation of the potential energy as the function of angles instead of bonds and thereby taking a step toward potential energy surfaces.
During the calculations related to H_3^-, the concept of computational cost became clear. Although the anion is a relative small molecule, the optimization of the first excited state using CCSDT and the aug-cc-pVQZ basis set took three days and only converged when the initial guess of the geometry was linear. Therefore, it has to be kept in mind that

the election of a larger basis set in order to obtain more accurate results implies a higher computational cost. The scaling behavior, or in other words the measure of computational cost is given by N^4 for HF, N^5 for MP2 and N^8 for CCSDT, being N the size of the basis set[9]. Instead of simply increasing N, the before mentioned extrapolation to the complete basis set (CBS) could be performed to improve the numeric results.
Regarding the outcomes obtained with Hückel's model, it can be said that the model gives a good overview on the energy level configuration and electron densities, without contradictions. However, the rough approximations, such as setting the overlap equal to zero in every case, have to be treated with caution.

A Sample Input File

```
memory heap 200 mb stack 1000 mb global 2800 mb
start H3_cation_ex_E1
echo
charge 1
geometry units au
symmetry C1
H     0.0    0.0    0.0
H     2.45    0.0    0.0
H    -1.50    0.0    0.0
end
basis
    H library aug-cc-pVQZ
end
scf
   rohf
   maxiter 5000
   triplet
   nopen 2
end
tce
   scf
   ccsdt
   diis 10
   maxiter 5000
end
task tce energy
```

Bibliography

[1] T. Oka. "Interstellar H_3^+". In: *Proc. Natl. Acad. Sci. USA (PNAS)* 103 (2006), pp. 12235–12242. URL: https://doi.org/10.1073/pnas.0601242103.

[2] T. Oka. "Chemistry, astronomy and physics of H_3^+". In: *Phil. Trans. R. Soc. A.* 370 (2012), pp. 4991–5000. URL: https://doi.org/10.1098/rsta.2012.0243.

[3] H. Kragh. "The childhood of H_3 and H_3^+". In: *Astronomy & Geophysics* 51 (2010), pp. 6.25–6.27. URL: https://doi.org/10.1111/j.1468-4004.2010.51625.x.

[4] J. Pelley. "Probing the Universe with H_3^+". In: *ACS Central Science* 5 (2019), pp. 741–744. URL: https://doi.org/10.1021/acscentsci.9b00441.

[5] W. Wang et al. "Observations of H_3^- and D_3^- from dielectric barrier discharge plasmas". In: *Chemical Physics Letters* 377 (2003), pp. 512–518. URL: https://www.sciencedirect.com/science/article/pii/S0009261403012107.

[6] L. Huang et al. "Anionic hydrogen clusters as a source of diffuse interstellar bands (DIBs)". 2019. URL: https://arxiv.org/abs/1912.11605.

[7] G. Herzberg. "A spectrum of triatomic hydrogen". In: *The Journal of Chemical Physics* 70 (1979), pp. 4806–4807. URL: https://doi.org/10.1063/1.437272.

[8] M. Tashiro and S. Kato. "Quantum dynamics study on predissociation of H_3 Rydberg states: Importance of indirect mechanism". In: *The Journal of Chemical Physics* 117 (2002). URL: http://dx.doi.org/10.1063/1.1490918.

[9] C. J. Cramer. *Essentials of Computational Chemistry*. 2nd ed. John Wiley & Sons, 2004.

[10] P. Atkins and R. Friedmann. *Molecular Quantum Mechanics*. 5th ed. Oxford University Press, 2011.

[11] D. Sherrill. "An Introduction to Hartree-Fock Molecular Orbital Theory". 2000. URL: https://dokumen.tips/documents/c-david-sherrill-an-introduction-to-hartree-fock-molecular-orbital-theory.html.

[12] F. Jensen. *Introduction to Computational Chemistry*. 2nd ed. John Wiley & Sons, 2007.

[13] K. Raghavachari et al. "A fifth-order perturbation comparison of electron correlation theories". In: *Chemical Physics Letters* 157 (1989), pp. 479–483. URL: https://www.sciencedirect.com/science/article/pii/S0009261489873956.

[14] T. H. Dunning. "Gaussian basis sets for use in correlated molecular calculations. I. The atoms boron through neon and hydrogen". In: *The Journal of Chemical Physics* 90 (1989), pp. 1007–1023. URL: https://doi.org/10.1063/1.456153.

[15] K. L. Schuchardt et al. "Basis Set Exchange: A Community Database for Computational Sciences". In: *Journal of Chemical Information and Modeling* 47 (2007), pp. 1045–1052. URL: https://www.basissetexchange.org/.

[16] E. Aprà et al. "NWChem: Past, present, and future". In: *The Journal of Chemical Physics* 152 (2020), p. 184102. URL: http://dx.doi.org/10.1063/5.0004997.

[17] "NWChem User Documentation". 2021. URL: https://nwchemgit.github.io/Home.html.

[18] A. Aguado et al. "Three states global fittings with improved long range: singlet and triplet states of H_3^+". In: *Phys. Chem. Chem. Phys.* 23 (2021), pp. 7735–7747. URL: http://dx.doi.org/10.1039/D0CP04100A.

[19] A. Mohammadi et al. "Coupled Cluster and Quantum Monte-Carlo study of anionic hydrogen clusters H_n^- $(3 \leq n(odd) \leq 11)$". In: *Chemical Physics Letters* 744 (2020), p. 137216. URL: https://www.sciencedirect.com/science/article/pii/S0009261420301317.

[20] M. Pavanello and L. Adamowicz. "High-accuracy calculations of the ground, 1^1A_1, and the 2^1A_1, 2^3A_1, and 1^1E_1 excited states of H_3^+". In: *The Journal of Chemical Physics* 130 (2009), p. 034104. URL: https://doi.org/10.1063/1.3058634.

[21] C. Sanz et al. "The lowest triplet state ^3A of H_3^+ Global potential energy surface and vibrational calculations". In: *The Journal of Chemical Physics* 114 (2001), pp. 2182–2191. URL: http://hdl.handle.net/10261/72453.

[22] O. Chuluunbaatar et al. "D_{3h} symmetry adapted correlated three center wave functions of the ground and the first five excited states of H_3^+". In: *Chemical Physics Letters* 746 (2020), p. 137304. URL: https://www.sciencedirect.com/science/article/pii/S0009261420302190.

[23] B. Brandsen and C. J. Joachain. *Physics of Atoms and Molecules*. John Wiley & Sons, 1983, p. 140.

[24] Z. Peng et al. "Excited electronic potential energy surfaces and transition moments for the H_3 system". In: *Physical Review A* 52 (1995), pp. 1005–1023. URL: https://doi.org/10.1103/PhysRevA.52.1005.

[25] J. C. Rayez et al. "Theoretical study of the H_3^- cluster". In: *The Journal of Chemical Physics* 75 (1981), pp. 5393–5397. URL: https://doi.org/10.1063/1.441939.